international
Nonwovens
Journal

A Science and Technology Publication

Volume 9, No. 3 **Fall, 2000**

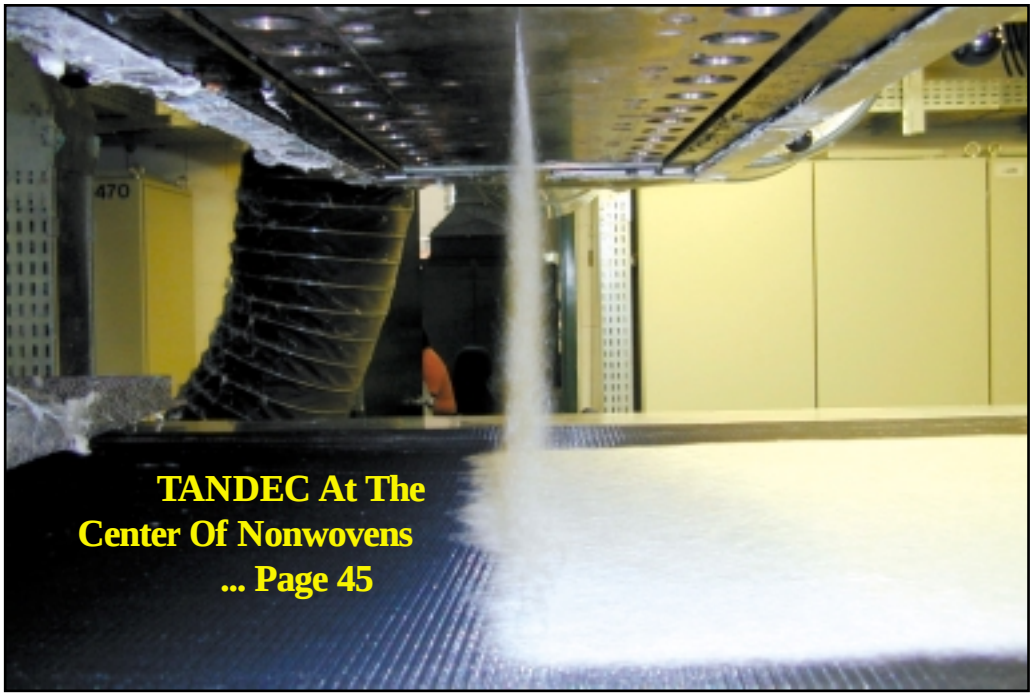

Special INTC 2000 Issue

September 26-28, 2000, Dallas, Texas

international Nonwovens Journal

A Science and Technology Publication

Vol. 9, No. 3 ***Fall, 2000***

The International Nonwovens Journal Mission: To publish the best peer reviewed research journal with broad appeal to the global nonwovens community that stimulates and fosters the advancement of nonwoven technology.

Cover Photo courtesy of TANDEC, University of Tennessee

THE DIRECTOR'S CORNER

Laboratory Safety

A laboratory is not the riskiest place in the world. On the other hand, a laboratory is not the safest place in the world either. Making a laboratory a safer place in which to work is primarily the responsibility of the research administrator, but everyone involved must consider it to be their responsibility as well. In addition, of course, it is an activity which is subject to government oversight.

The "Laboratory Standard" is the OSHA standard to which laboratories in the United States must adhere. This is actually OSHA Standard 29 CFR 1910.1450. Laboratories covered by this standard according to the OSHA definition are facilities where relatively small quantities of hazardous chemicals are used on a non-production basis. Quality control labs and other laboratories that perform routine, standardized tests that monitor and support production processes are not covered by this standard; they are considered adjuncts of production operations. Also, facilities such as dental or photographic labs are considered production facilities and are covered under the hazard communication standard, but not OSHA's lab standard.

Laboratories that conduct research and development and related analytical work are subject to the requirements of the "Laboratory Standard." According to OSHA data, the Federal laboratory standard covers approximately 934,000 employees in 32,214 industrial, clinical and academic laboratories.

The situations, materials and environments that are considered to be a hazard by this standard include the following:

- Hazardous chemicals
- Substances of high toxicity
- Bio-hazardous and radioactive materials
- Flammable chemicals
- High reactive or explosive chemicals
- Compressed gases
- Water cooled equipment
- Electrically powered laboratory equipment
- High/low pressures and temperatures
- Laboratory animals
- Infectious diseases

While a researcher may think a specific laboratory is not involved in hazardous materials, an examination of the list shows that almost any research laboratory that has much flexibility in its work capability has one or more items on the list.

Further, the following review of the 10 most frequent OSHA violations encountered in the research laboratory may cause the researcher to pause and think more seriously about the environment within the laboratory.

1. Occupational exposure, hazardous chemicals in the laboratory
2. Methylene chloride
3. Respiratory protection
4. Electrical, wiring methods, components and equipment
5. Personal protective equipment, general requirements
6. Hazard communication
7. Flammable and combustible liquids
8. Electrical systems design, general requirements
9. Means of egress, general requirements
10. Control of hazardous energy, lockout-tagout.

Certainly a well-managed research laboratory should not be a dangerous environment. Statistics on injury/illness rate indicate, that such locations have a fairly good record, particularly as compared to other work environments, as borne out by the data in *Table 1.*

While such statistics confirm the concept that the laboratory is not an unwarranted dangerous environment, it is incumbent upon every research administrator and person associated with the research laboratory to maintain vigilance and continually review places and practices, to insure the existence of "Prudent Practices" as suggested by the National Research Council; these should certainly be the guiding principle for all individuals involved *(Table 2).*

Table 1
1998 INJURY/ILLNESS INCIDENT RATE

Total Cases
Research & Testing Services: 2.5 cases per 100 full-time workers
Manufacturing Average: 9.7 cases
Private Industry Average: 6.7 cases
Chemical & Allied Products Average: 4.2 cases

Lost-workday Cases
Research & Testing Services: 1.0 cases per 100 full-time workers
Manufacturing Average: 4.7 cases
Private Industry Average: 3.1 cases
Chemical & Allied Products Average: 2.1 cases

(Source: Bureau of Labor Statistics)

On-Line Complaints

Almost everything can be done on-line these days, so why not complaints. At least that's the way OSHA (Occupational Safety and Health Administration) feels about complaints from workers. As a result, workers can now use the Internet to file complaints about safety and health hazards at their workplaces. This move was apparently promptly by the growing number of Americans who have Internet access and their willingness to conduct business electronically. "The worker's page" will be an on-line resource that gives employees an electronic option for filing formal complaints. Previously, employees had to either call or write OSHA when alleging workplace hazards.

As one of the OSHA officials indicated, "workers play a vital role in identifying workplace hazards, and whenever

Table 2
PRUDENT PRACTICES

1. *Minimize all chemical exposures.* Because few laboratory chemicals are without hazards, general precautions for handling all laboratory chemicals should be adopted, rather than specific guidelines for particular chemicals. Skin contact with chemicals should be avoided as a cardinal rule.

2. *Avoid underestimation of risk.* Even for substances of no known significant hazard, exposure should be minimized; for work with substances that present special hazards, special precautions should be taken. Assume that any mixture will be more toxic than its most toxic component, and that all substances of unknown toxicity are toxic.

3. *Provide adequate ventilation.* The best way to prevent exposure to airborne substances is to prevent their escape into the working atmosphere, by use of hoods and other ventilation devices.

4. *Institute a Chemical Hygiene Program.* A mandatory chemical hygiene program designed to minimize exposures is needed. It should be a regular, continuing effort, not merely a standby or short-term activity.

5. *Observe the PELs and TLVs.* The Permissible Exposure Limits of OSHA and the Threshold Limit Values of the American Conference of Governmental Industrial Hygienists should not be exceeded.

(Source: National Research Council)

possible, working with their employers to correct them and many times employers will promptly fix the hazards, but if they don't, workers can file a complaint with OSHA by telephone, fax, letter or now electronically through out website."

Once at the website (www.osha.gov) workers will find an easy-to-use system that requires complaints to be entered into a few fields of information, including their name and telephone number and the employers name, a description of the hazard and its location. OSHA estimates that it takes about 10 minutes to complete the on-line complaint form and send it. The form is automatically transmitted for follow-up to the appropriate OSHA office within the complainant's state.

All on-line complaints are investigated and many can be resolved informally, usually by telephone and fax with the employer. Complaints not informally resolved are likely to result in on-site inspections of the facilities by OSHA. The Occupational Safety and Health Act of 1970 gives employees the right to file complaints about workplace safety and health hazards. The Act gives the complainants the right to request that their names not be revealed to their employers.

Hidden Employee Costs

In addition to the obvious employee costs of salaries and various benefits, there are some costs that are significant, but may be somewhat hidden, especially if an organization does not want to recognize them.

Two of these significant costs that may be buried from view are employee absenteeism and employee turnover.

In the United States, employee absenteeism traditionally runs between 1.5 and 2%. Special situations can cause this to rise, of course, but this does provide a good benchmark. Deviation from this norm should raise a "red flag" that results in some study of individual situations.

Over the past five years, the turnover rate in the United States has risen, as might be expected in times of high employment. This rise has been from 13.6 to 17.8% for non-exempt employees, and from 9.9 to 12.5% for exempt employees.

One employment specialty company points out that the average revenue generated per employee is $985 per day. If it takes about two months to fill the average job, a company has lost about $60,000.

Again, these figures may vary from company to company, but the principle is the same — keep an eye on hidden employee costs!

Fewer U.S. Science and Engineering Graduates

With the widespread publicity on the necessity for youth to obtain a full education in order to be an effective employee/citizen/participant/wage-earner in the 21st Century Digital Age, it is rather surprising to consider the actual situation.

U.S. students' interest in careers in engineering continues to decline. This is shown by the number of Bachelor's degrees granted in all kinds of engineering — it reached a 10-year low in 1999. The study confirming this situation involved 20 fields, including electrical, biomedical, chemical, materials and metallurgical engineering. The number of degrees in Chemical Engineering, which had been increasing slower, fell for the first time in nearly a decade; this discipline seemed to peak in 1997.

Data from the National Science Foundation shows that the U.S. ranks 19th in the world in the number of science and engineering graduate students among its population of 24 year olds *(Table 3).— **INJ***

Table 3
ENGINEERING DEGREE RANKING

Rank	Country	Degrees
1	Georgia	11.0
2	Russia	10.2
3	Finland	9.9
4	United Kingdom	9.4
5	South Korea	8.9
6	Germany	8.1
7	Australia	8.0
8	Singapore	7.8
9	Ireland	7.5
10	Japan	7.2
19	United States	5.4

RESEARCHER'S TOOLBOX

Out-Sourcing Laboratory Testing

In this day of downsizing and focusing on core business, some traditional business services are best handled on an out-sourcing basis. This involves the routine use of outside organizations to handle internal and continuing obligations and responsibilities.

The out-sourcing of laboratory service work has been practiced to a limited extent in the past. However, with new capabilities and conveniences centered on the Internet, this method of getting more done with less may become more important.

Smithers Scientific Services, Akron, Ohio, may have taken this possibility to a new height. The company has launched a new, interactive web site for customers and prospects wishing to use its polymer products testing laboratories. Clients now have the ability to browse the extensive testing services and capabilities of this organization.

This "browsing" system includes video footage and hundreds of laboratory pictures to walk the user through various laboratories and testing services offered by Smithers. This includes a CD-ROM for reviewing the laboratory facilities, as well as viewing the accreditation received by the laboratory. Their website also provides links to informational and test specification sites in addition to the accreditation organization sites. If Smithers is not in a position to provide a specific test capability, their site does give links to alternative sources for such testing, through their Test Source Locator.

The mini disk also provides a means for accessing the laboratory price-quoting system. This is coupled with an on-line request system for an instant quotation on a specific testing job. This further allows an examination of the laboratory testing schedule, in order to have insights into the anticipated response dates. For more information: Smithers Scientific Services, 425 West Market, Akron, OH 44303; 330-762-7441; www.smithersquote.com).

Another commercial testing laboratory has begun to offer some scientific services that may prove useful in the out-sourcing process. This is Worldwide Testing, headquartered in Atlanta, Georgia, with an office in Houston, Texas. This system is a little different, in that it brings together customers that want testing with a group of testing laboratories seeking such clients.

This service claims to use a patent-pending method for allowing buyers and sellers to access secure laboratory sample and test data relating to products that are offered through trading exchanges and on-line catalog sales.

Worldwide Testing has a process for qualifying the 25 laboratory partners for their analytical capabilities, areas of testing expertise, size of technical staff and equipment. This qualification process requires each qualifying laboratory to have in place a quality system that satisfies a nationally or internationally recognized accreditation or certification standard, such as ISO Guide 25, ISO 9002, A2LA or MAVALP. This assures the customer can have confidence in the test results obtained.

Some of the laboratory partners are qualified for pharmaceutical testing according to the United States pharmacopeia, British pharmacopeia, Japanese pharmacopeia and other European pharmacopeia, along with meeting the requirements for Good Laboratory Practices (GLP). For more information: Worldwide Testing, 7000 Central Parkway, Suite 1550, Atlanta, GA 30328; 770-225-5500; www.worldwidetesting.com.

Yet another organization offering scientific measurements and services to customers is LabSeek.com. Their activities are limited to the internet, but on a worldwide basis. The company is located in Minneapolis, Minnesota, and provides outsourced analytical chemistry problem solving and testing services to a wide range of customers.

Recently, three European labs (Lareal in France, Chemalys in Sweden, and Calipso of the Netherlands) joined. LabSeek. Previous labs covered by this service include 35 labs in North America, including BP, Pace Analytical Services, Phillips Petroleum, Shell Chemical and Ticona Chemical. For more information: www.labseek.com.

* * *

Another interesting testing activity available to the nonwovens industry is the offering by the U.S. Army Soldier System Center, Natick, Massachusetts for use of its Doriot Climatic Chambers facility.

The equipment included in this facility includes both arctic and tropic wind tunnels, with wind, rain, solar temperature and relative humidity features. With the ability to simulate rain up to four inches per hour and a wind environment up to forty miles an hour, the chambers provide extreme climate testing. Temperatures inside the chamber can be controlled to within 1^0 F, within the range from -70^0 F to 165^0 F. For more information: U.S. Army Soldier System Center, Kansas Street, Natick, MA 01760; 508-233-5295; jane.simpson@natick.army.mil: www.sbccom.army.mil)

Validation and Quality In The Laboratory

A new partnership may make it easier for a laboratory to achieve accreditation on a national scale. By establishing national standards for the accreditors, a laboratory may more easily validate its qualifications to meet all of the federal, state, local and specialty requirements.

This should be accomplished by a partnership between the National Institute of Standards & Technology (NIST) and the National Cooperation for Laboratory Accreditation (NCLA). NIST is the old NBS (National Bureau of Standards); NCLA is a private organization of lab accreditors.

This agreement should also facilitate U.S. labs meeting international accreditation programs. (www.ts.nist.gov).

* * *

Three recent publications deal with the implementation of a quality system in the

laboratory, along with validation of analytical methods.

1. "Step-by-step implementation of quality system in the laboratory," by Maria Joã O. Benoliel (Empresa Portuguesa das Aguas Livres ASA). Laboratorio Central da EPAL, rua do Alviela 12, P-1170-012 Lisboa Codex, Portugal), Transanalytical Chemistry, 18 9-10: 632-638 (1998).

In recent years laboratories have undergone huge transformations due to the technological development of inspection and testing equipment; the introduction of computerized and automated systems; keen competitiveness between companies/laboratories as a result of demand within Europe and on the international market; and greater consumer awareness of the quality of the products available. Laboratory accreditation, though a voluntary process, is formal recognition by an accreditation body of the laboratory's competence to carry out certain tests. This article presents these aspects that should be taken into account in the step-by-step implementation of a quality system and also makes reference to the requirements of accredited laboratories in accordance with European standard EN45001.

2. "Inter-laboratory, time, and fitness-for-purpose aspects of effective validation," by Hilko van der Voet, J. A. (Hans) van Rhijn and Henk J. van de Wiel (Centre for Biometry, Wageningen, P.O. 16, 6700 AA Wageningen, Netherlands). Analytica Chemica Acta, 391 2:159-171 (1999).

This paper reviews current approaches to validation in analytical methods. It identifies some shortcomings of existing validation schemes, such as insufficient coverage of variability in space or time and mismatches between validation criteria and intended use of the method, e.g., the use of regulatory control.

A general statistical modeling approach for combining different aspects of validation is recommended, and illustrated with an example. This type of modeling, based on components of variation, is advocated as a basis for the development of new statistically underpinned validation schemes that integrate current validation and quality assurance activities.

3. "How to validate analytical methods," by Roger Wood (Food Contaminants Division, Joint Food Safety and Standards Group, Ministry of Agriculture, Fisheries and Food), Institute of Food Research, Norwich Research Park, Colney, Norwich NR4 7UQ, UK.(Tel: 44+1603/255-000; r.wood@ffcii.maf.gov.uk), Trends and Analytical Chemistry, 18, 9-10:624-632 (1999).

The requirement for laboratories to use a "fully validated" method of analysis is now accepted or required in many sections of analysis. Fully validated means that a method must have been assessed in a collaborative trial. The significance of these requirements is described because analysts will increasingly will be required to justify their choice of method in light of them. In addition, the requirements and procedures that may be used to obtain methods that have been validated "in-house," without full validation through collaborative trial, are also outlined in the article; these point the way to international acceptance of such methods in the future, as the cost of carrying out full validation of methods through collaborative trials becomes prohibitive.

* * *

Besides lab certification, there is certification for the laboratory technician. A recent program inaugurated by AATCC (American Association of Textile Chemists and Colorists) provides a Certification Program for "Textile Technologists." This program is designed to ensure competency on the part of textile laboratory technologists with respect to specific textile laboratory tests. The initial test modules cover a variety of color, colorfastness and related tests.

Qualification is based on obtaining a minimum score on a written test and demonstrating competency in the testing laboratory, following completion of a training course. Also, a series of samples are evaluated in the technician's home laboratory to establish transfer of the competency to the normal surroundings. (For more information: Peggy Picket, AATCC, Research Triangle Park, NC 27790; 919-549-3533; www.aatcc.org.)

Improved Polymer Characterization

At times it is necessary to analyze a polymer very accurately in order to provide correlation of molecular properties to the resulting product properties and performance.

Molecular weight distribution is a critical factor in the performance of many polymers, as it may be tied to melt viscosity and other properties that are important both during processing and in the performance of the end product. The use of conventional size exclusion chromatography (SEC) to determine molecular weights may not be accurate for considerable research and development work, because the broad molecular weight distribution of many polymers makes it difficult to match with the standard. Also, the use of highly polar solvents for the polymer may result in the polymer reacting with the packing, with the result that separation is not based exclusively on size; when this happens, exact molecular weights cannot be obtained.

These problems have been solved with a souped-up version of SEC resulting in a new polymer tool, SEC3. In this system, the SEC capability is combined with a laser light-scattering detector, a refractive index detector and a viscometer to accurately characterize molecular weight, size and branching of the polymer. This enhanced capability permits the analysis of polymers with very accurate results, which can the research correlate molecular properties to a variety of other downstream characteristics.

This instrument enhancement, which was done by DuPont researchers, involved reconfiguring an instrument that contained dual viscosity and light-scattering detectors, by adding an RI detector and an autosampler. The unit was integrated in such a manner that polymer molecules elute from the SEC columns and are monitored simultaneously in real time by all three detectors. The ability to measure molecular weight distribution far more accurately than in the past has helped researchers correlate physical property to molecular structure with a higher degree of certainty. (For more information: David E. Niehaus, DuPont Experiment Station, B228, Room 238A, Wilmington, DE; 302-695-9578). ***— INJ***

ABSTRACTS AND REVIEWS

A sampling of Nonwovens Abstracts from Pira International — A unique intelligence service for the nonwovens industry

Hollow fibres from hybrid polymers

Ormocers are hybrid polymers whose molecular structure contains both glass-like inorganic and organic sections. They are prepared by thermal, ultraviolet or light induced polymerisation of multifunctional silanes. A novel process by which such polymers can be spun into hollow fibres is described. The ormocer hollow fibres can then be pyrolysed to create hollow silicon dioxide fibres. (11 fig, 2 tab, 8 ref)

Author: Ballweg T; Wolter H

Source: Gummi Fasern Kunstst.

Issue: vol. 53, no. 4, Apr. 2000, pp 277-281 (In German)

Overseas topics: business improvement in the nonwoven car interior industry, supported by the active car industry in the USA

The nonwoven car interior business was predicted to record 10% growth in 1999, supported by the active car industry in the U.S. Nonwoven sales in the car industry was 310m sq yard (excluding carpet base, filter and composite applications) in 1998, which was $180 million. The impact of material recyclability in the USA is not as strong as in Europe; however, material recycling is believed to be the key issue in the future as most car manufacturers are multinational. The nonwoven from natural materials, exhibited in Detroit Automotive Show (Jan. 2000), has a high market potential because of its lightweight, cost efficiency and recyclability. (1 ref)

Author: Anon

Source: Jpn Nonwovens Rep.

Issue: no. 314, 10 Apr. 2000, pp 54-56 (In Japanese)

Materials recycling

Focusing on the German automotive sector, current and possible future trends in the recycling of thermoplastic materials and composites containing thermoplastics are discussed. Styrene polymers, polyolefins, polyamides and polyphenylene ether blends and styrene maleic anhydride offer the greatest potential for numerous reuse. (1 fig, 2 tab)

Author: Wiedemann P

Source: Kunstst. Plast Eur.

Issue: vol. 90, no. 2, Feb. 2000, pp 21-23e, pp 65-70d

Issue: vol. 43, no. 2, May 2000, p. E28

Sandler: melt-blown nonwovens

Sandler, Schwarzenbach Saale, Germany, has devised a way of producing nonwovens directly from granulate polymer. A series of hygiene and filtration products has been introduced under the "sawascreen" brand. Hydrophobic, hydrophilic, bacteriostat and antimicrobial composites are also available. Performance and properties of hygiene nonwovens are greatly improved by the new technology. Voluminous nonwoven filters have excellent dust holding capabilities, meeting F6-F9 filter class requirements, and being economically efficient. (Short article)

Author: Anon

Source: Tech. Text.

Issue: vol. 43, no. 2, May 2000, p. E28

Characteristics of needle-punched nonwoven and needle selection

Foster Needle Co Inc. introduced their advanced needle technology and products. Four parameters of felt needles decide the quality and characteristics of needlepunched nonwoven: blade shape (triangular, star and pinched shape); barb shape (formed, untreated and open); barb interval; needle length. (9 fig, 1 tab)

Author: Tsubaki S

Source: Jpn Nonwovens Rep.

Issue: no. 313, 10 Mar. 2000, pp 4-9 (In Japanese)

100% web inspection

Modular optical film, nonwoven and paper web inspection systems comprise one or more CCD line cameras. A 2500mm wide film running at 150m/min will generate 25MB of data/s. Intelligent web sensors enable only production-relevant data to be selected for transmission to database computers. This data is stored and can generate graphs or tables for operators. (2 fig)

Author: Krampe R

Source: Kunstst. Plast Eur.

Issue: vol. 90, no. 4, Apr. 2000, pp 30-31e, 84-86d

Studies on dyeing with natural dyes: part II – dyeing of berberine on acrylic fibre

Berberine is the only known natural basic dye, but the berberine base is unstable and assumes the aldehyde from berberinal, whereas its salts are derived from the ammonium form. Acrylic staple fibres were used for kinetic and thermodynamic studies of the mechanisms of dyeing such fibres with berberine. (4 fig, 2 tab, 1 ref)

Author: Gulrajani M L; Gupta D; Maulik S R

Source: Indian J. Fibre Text. Res.

Issue: vol. 24, no. 3, Sept. 1999, pp 223-225 ***— INJ***

These pages feature an extract from Nonwovens Abstracts, compiled by Pira International from international business journals, newspapers, market research reports and conference proceedings.

Comparison of Electrostatic Charging at Different Locations In The Melt Blowing Process

By Peter Ping-yi Tsai, Guo-wei Qin and Charles Hassenboehler, TANDEC-Textiles and Nonwovens Development Center, The University of Tennessee, Knoxville, TN

Abstract

Melt blown (MB) fabrics are composed of fine fibers which contribute to high filtration efficiency (FE) and low air flow resistance compared to high efficiency filtration media such as fiber glass paper. Furthermore, MB fabrics are mostly made of polypropylene (PP) polymer, which can be electrostatically charged to enhance the media filtration efficiency without the increase of air flow resistance. However, different charging techniques or charging at different locations on the MB line will contribute to different filtration efficiency. This paper compares the efficiencies of different charging techniques in the MB line.

Keywords

Electrostatic charging, melt blown webs, charging techniques, filtration efficiency, filters.

Melt blowing is a one-step process to make a nonwoven fabric from polymer chips through fiber spinning [1]. Fine fiber diameters of 1.5 mm to 2 mm can be produced. Fine fibers take the advantage of high surface area that contributes to high FE by mechanical mechanisms [2]. MB PP webs can be electrostatically charged to increase the FE by electrical attraction mechanisms [3] without the increase of air flow resistance. Fibrous materials can be electrostatically charged by several methods such as polarization, induction, triboelectrification and corona charging. Electrets made by polarization and induction are not suitable for filters. But, triboelectrification is a good process that can charge the media to a high FE [4]. However, this technique requires two types of fibers having different electronegative properties. Corona charging is the only technique to electrostatically charge the fibers or fabrics in the MB process. The corona discharge theory and the corona charging techniques applied on MB line have been reviewed by Tsai, et al [5]. This paper compares the FE improved by corona charging of MB fibers or webs at different locations in the MB process for different basis weights.

Experimental

Three basis weights, low (20 g/m^2), medium (35g/m^2) and high (100g/m^2), were produced by the Accurate Products Accuweb System 20-inch MB line at the University of Tennessee, shown in *Figure 1*. The fibers or fabrics were charged at locations A, B, C, D and E using Simco's high-voltage power supplies.

In location A, a thin wire of 0.15 mm in diameter was placed in the center between the walls of the air path having a spacing of 1.5 mm. The wire was electrically insulated by a ceramic ring at the end of the die body. The wire was subjected to a positive or a negative high voltage while the die body was grounded. The fibers were charged at the die exit when they were in a semi-molten stage by aerodynamic force from the MB primary air that carried the corona discharges generated around the wire.

In location B, two rows of pins were attached on the top

Figure 1
EXXON MELT BLOWING PILOT LINE AT THE UNIVERSITY OF TENNESSEE AND CORONA CHARGING LOCATIONS IN THE LINE

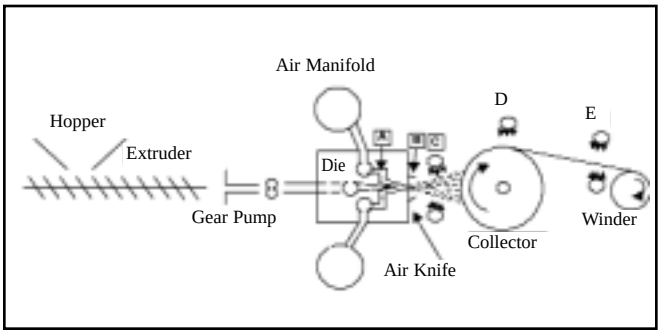

and bottom air knives, respectively. The spacing between two pins was 1.27 cm. Two solid bars, each having a diameter of 2.54 cm, were located 3.7 cm away from the center line of the air gap and also 3.7 cm from the air knife measured from the center of the bar. The bar was subjected to positive or negative high voltage while the pins were grounded with the die body. The fibers were charged at the die exit when they were still in molten stage by electric field force or by aerodynamic force.

In location C, two wires having a diameter of 0.15 mm each were separated by 5 cm, and 5 cm away from the die body. The electric field was created between the two wires when they were subjected to opposite polarities of high voltages. The fibers were charged when they fly between the wires while they were still hot or in a semi-molten stage. Voltages with the same polarities can be simultaneously applied to both wires while the die body was grounded. Therefore, the electric field was created between the wire and the die body. Fibers were charged between the wires and the die body when they were in a molten or semi-molten stage. Two Simco charging bars with point emitters were tried in place of the wires. However, success was not achieved because the bars were deflected by the air flow.

In location D, a wire having a diameter of 0.2 mm was placed 5 cm above the collector, which is made of stainless wire screen. The wire was subjected to positive or negative voltage while the collector was grounded. The fabric was charged on the collector by electric field force while the fibers were solidified but still hot or warm.

In location E, two methods were employed. Method 1 had two wires, each having a diameter of 0.2 mm, 5 cm apart, and two Simco's charging bars, 5 cm pin-to-pin apart. The wires or the bars were subjected to opposite polarities. The fabrics were charged by electric field force when they passed between the wires or the bars. The fibers in the webs had reached room temperature when they traveled to the charging area. Method 2 in location E was "Tantret," technology developed at the University of Tennessee [6]. It has two techniques, Tech-I and Tech-II. Tech-I is a wire having a diameter of 0.2 mm located 2 inches above a biased steel roll having a diameter of 2 inches. A positive or negative voltage was applied to the wire while the roll was biased by an opposite polarity of voltage. The fabric was charged by electric field force while it contacted with the roll. Tech-II consists of a wire having diameter of 0.2 mm located in the center of a shell having a diameter of 7 inches. Dielectric rolls were installed between the wire and the shell to support the fabric when it travels through the shell during the charging process. These two techniques are both effective in charging the room-temperature fabrics. However, because of their mechanical structure they are not eligible to charge the fibers before the fabrics are formed in Location D, *Figure 1*.

After charging, surface charge potential and FE were measured. Surface charge potential was measured using a scanning system designed at the University of Tennessee, as shown in *Figure 2*. The system consists of a scanning table which carries a capacitive probe having an aperture of 1.78 mm from Monroe Electronics to move along X- and Y- directions at a predetermined interval. One side of the fabric was facing the probe aperture while the other side was grounded. An electrometer used to measure the voltage from the probe and the data were interfaced with the computer for statistical analysis.

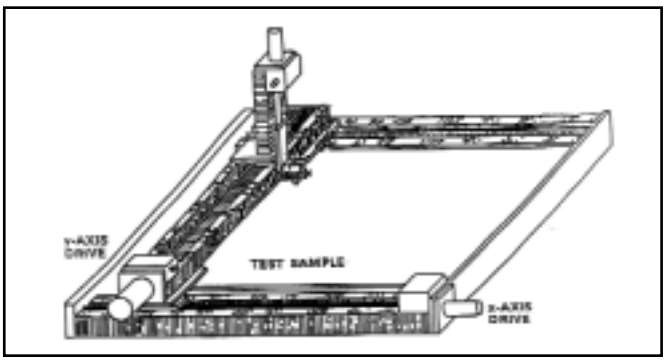

Figure 2
SURFACE CHARGE POTENTIAL MEASURING SYSTEM DEVELOPED AT UT-TANDEC

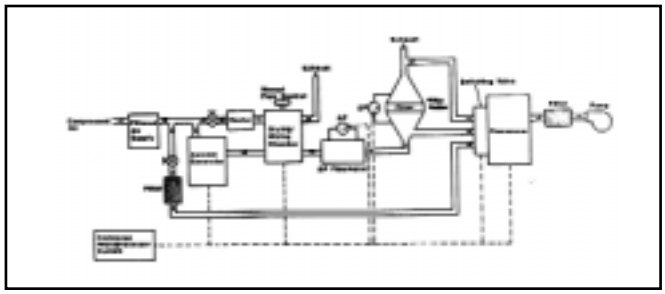

Figure 3
SCHEMATIC DIAGRAM OF NaCl FILTRATION TESTER (COURTESY OF TSI INC., ST. PAUL, MN)

Two filtration testings were performed using a TSI 8110 for NaCl particle FE and a latex tester to simulate the bacteria FE [7]. A filtration tester is consisted of two major components, aerosol generator and particle detector. *Figure 3* is the schematic diagram of the NaCl filtration tester. The particle detector in this tester is a photometer, which measures the aerosol volume concentration, and an optical particle counter in the latex filtration tester, which measures the aerosol number concentration. The NaCl particle had a number average diameter of 0.067 μm with a standard deviation of 1.9 at an aerosol face velocity of 5.3 cm/s. The latex had a particle size of 0.8 μm with a monodisperse particle size distribution at an aerosol face velocity of 1.1 cm/s.

Results and discussion

A randomly distributed positive and negative charge potential was measured on both sides of the fabric charged at location A. *Figure 4* shows the surface charge potential plot on the face side of Sample number 2 in *Table 1* while the surface charge potential on the screen side of the fabric is shown in *Figure 5*. The charging conditions and the testing results of the fabrics charged at location A are shown in *Table 1*. Fabrics

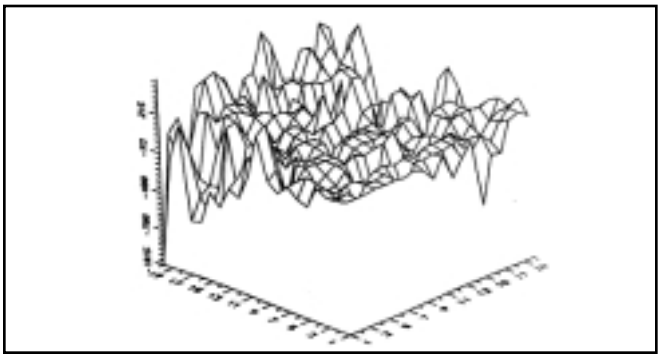

Figure 4
SURFACE CHARGE POTENTIAL OF THE FACE SIDE OF A 35 G/M^2 FABRIC CHARGED AT LOCATION A IN THE MELT BLOWING PROCESS

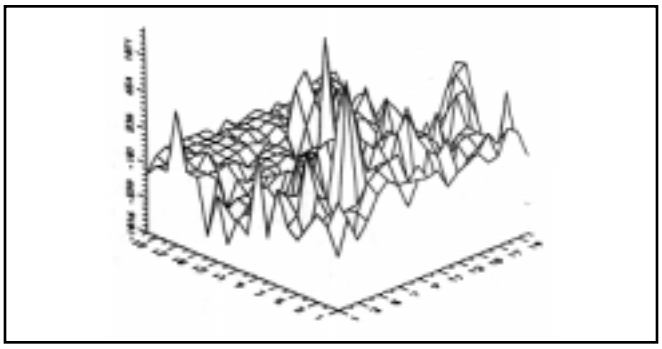

Figure 5
SURFACE CHARGE POTENTIAL ON THE SCREEN SIDE OF THE FABRIC IN FIGURE 4

of different basis weights charged in location A had the same trend of positive and negative charge potentials randomly distributed across the fabrics. A lower amount of surface charge potential was measured by this charging technique because the randomly distributed positive and negative charges cancelled each other. A latex FE of 96% and NaCl FE of 70% for the 35 g/m^2 fabric could be achieved by this technique. Both positive or both negative voltages on the wire did not make difference in the FE. Strangely, the positive voltages on the wire charged the fabrics to a negative surface potentials while the negative voltage charged to a positive surface charge potentials. However, positive voltage on one wire and negative voltage on the other wire charged the fabrics to a low surface charge potentials and low FE, not listed in the Table, because the positive and negative charges were neutralized at the die exit before they were embedded into the fibers. For the fabrics charged at location A, the increase of FE on both latex and NaCl by the increase of the basis weight basically obeys the following equation

$$p = e^{-\mu w} \quad \text{-------- (1)}$$

Where P = penetration
μ = filtration coefficient
w = basis weight
FE = 1 - P
Penetration is defined as

$$p = \frac{\textit{Downstream Aerosol Concentration}}{\textit{Upstream Aerosol Concentration}} \quad \text{---- (2)}$$

As can be calculated, the filtration coefficient (μ) was nearly constant for different basis weights of the fabrics charged in location A. This means that the ability to charge the fibers is not affected by the basis weight of the fabrics.

Table 1
SURFACE CHARGE POTENTIAL AND FILTRATION EFFICIENCY OF THE FABRICS MADE OF THE FIBERS CHARGED AT LOCATION A IN THE MELT BLOWING LINE WITH WIRES IN THE HOT AIR SLOTS

Sample Number	Basis Weight (g/m^2)	Charging Voltage (KV)	Surface Charge Potential (V)	Filtration Efficiency (%) Latex control	Latex charged	NaCl control	NaCl charged
1	20	+3.5	F*: -75 S**: -32	47	86.8	28	54
2	35	+3.5	F: -105 S: -54	65	96.3	38	72
3	100	+3.5	F: -134 S: -76	94	99.989	76	97.1
4	20	-3.5	F: +22 S: +10	47	85.2	28	53
5	35	-3.5	F: -48 S: +20	65	95.8	38	70
6	100	-3.5	F: +110 S: +115	94	99.986	76	98.2

* F = Face side of the fabric **S = Screen side of the fabric

Table 2

SURFACE CHARGE POTENTIAL AND FILTRATION EFFICIENCY OF THE FABRICS MADE OF THE FIBERS CHARGED AT LOCATION B IN THE MELT BLOWING LINE USING PINS ON THE AIR KNIVES

Sample Number	Basis Weight (g/m^2)	Charging Voltage (KV)	Surface Charge Potential (V)	Filtration Efficiency (%) Latex control	Latex charged	NaCl control	NaCl charged
1	20	+21	F*: -82 S**: -30	47	80.4	28	49.8
2	35	+21	F: -116 S: -48	65	93.2	38	68.2
3	100	+21	F: -157 S: -73	94	99.92	76	95.4
4	20	-21	F: +56 S: +25	47	81.2	28	48.9
5	35	-21	F: +115 S: +78	65	93.8	38	65.3
6	100	-21	F: +223 S: +157	94	99.89	76	94.8

* F = Face side of the fabric **S = Screen side of the fabric

The properties of the surface charge potentials and the FE of the fabrics charged in location B are similar to those charged in location A, as shown in *Table 2*. The only difference was that the positive bar voltages charged the fabrics to a negative surface charge potential while negative bar voltages charged the fabrics to a positive surface charge potential

Table 3

SURFACE CHARGE POTENTIAL AND FILTRATION EFFICIENCY OF THE FABRICS MADE OF THE FIBERS CHARGED AT LOCATION C IN THE MELT BLOWING LINE WITH WIRES SPACED 5CM APART

Sample Number	Basis Weight (g/m^2)	Charging Voltage (KV)	Surface Charge Potential (V)	Filtration Efficiency (%) Latex control	Latex charged	NaCl control	NaCl charged
1	20	Top: +21 Bottom: +21	F*: +121 S**: +98	47	89.8	28	58
2	35	Top: +21 Bottom: +21	F: +188 S: +142	65	97.6	38	78.1
3	100	Top: +21 Bottom: +21	F: +336 S: +255	94	99.994	76	98.2
4	20	Top: -21 Bottom: -21	F: -145 S: -112	47	87.2	28	57.6
5	35	Top: -21 Bottom: -21	F: -222 S: -189	65	96.8	38	76.3
6	100	Top: -21 Bottom: -21	F: -418 S: 1322	94	99.991	76	96.3
7	20	Top: +15 Bottom: -15	F: +118 S: -32	47	90.2	28	63.5
8	35	Top: +15 Bottom: -15	F: +175 S: -88	65	98.2	38	82.4
9	100	Top: +15 Bottom: -15	F: +339 S: -292	94	99.996	76	99.3

* F = Face side of the fabric **S = Screen side of the fabric

Table 4

SURFACE CHARGE POTENTIAL AND FILTRATION EFFICIENCY OF THE FABRICS CHARGED AT LOCATION D IN THE MELT BLOWING LINE USING A WIRE 5CM ABOVE THE COLLECTOR

Sample Number	Basis Weight (g/m^2)	Charging Voltage (KV)	Surface Charge Potential (V)	Filtration Efficiency (%) Latex		NaCl	
				control	charged	control	charged
1	20	+33	F*: +128 S**: -142	47	90.6	28	72
2	35	+33	F: +212 S: -226	65	98.2	38	87
3	100	+33	F: +315 S: -336	94	99.93	76	98.9
4	20	-33	F: -135 S: +112	47	89.4	28	69
5	35	-33	F: -224 S: +196	65	98.5	38	86
6	100	-33	F: -398 S: +322	94	99.96	76	99.1

* F = Face side of the fabric **S = Screen side of the fabric

because the pins are relatively negative for positive bars and relatively positive for negative bars.

The same trend for surface charge potentials and FE is true for the fabrics charged at location C, as shown in *Table 3*. However, the fibers were farther away from the die and they were more solidified when they were subjected to the charges. Therefore, the variation of the charge distribution both in polarities and magnitude was decreased and the FE was increased. A bipolar fabric was produced when charged by the wires with different polarities.

Fabrics charged at location D show a bipolar property, as shown in *Table 4*. The fabric FE was higher than those charged by the methods in the previous locations. However, the fabrics had been formed when they were being charged. Therefore, the FE increased at a slower rate with the increase of the basis weight in accordance with Equation 1. This

Table 5

SURFACE CHARGE POTENTIAL AND FILTRATION EFFICIENCY OF THE FABRICS CHARGED AT LOCATION E IN THE MELT BLOWING LINE

Sample Number	Basis Weight (g/m^2)	Charging Voltage (KV)	Surface Charge Potential (V)	Filtration Efficiency (%) Latex		NaCl	
				control	charged	control	charged
1	20	Top wire: +16 Bottom wire: -15	F*: +98 S**: -106	47	68	28	51
2	35	Top wire: +16 Bottom wire: -15	F: +142 S: -182	65	84	38	58
3	100	Top wire: +16 Bottom wire: -15	F: +222 S: -241	94	99.2	76	89
4	20	Top wire: -16 Bottom wire: +15	F: -112 S: +96	47	66	28	52
5	35	Top wire: -16 Bottom wire: +15	F: -178 S: +150	65	82	38	64
6	100	Top wire: -16 Bottom wire: +15	F: -245 S: +204	94	99.4	76	92

* F = Face side of the fabric **S = Screen side of the fabric

Table 6
SURFACE CHARGE POTENTIAL AND FILTRATION EFFICIENCY OF THE FABRICS CHARGEDAT LOCATION E USING TANTRET, TECH-I.

Sample Number	Basis Weight (g/m^2)	Charging Voltage (KV)	Surface Charge Potential (V)	Filtration Efficiency (%) Latex control	Latex charged	NaCl control	NaCl charged
1	20	wire: +38 roll: -1	F*: +158 S**: -172	47	96.5	28	92.2
2	35	wire: +38 roll: -1	F: +289 S: -312	65	99.6	38	97.8
3	100	wire: +38 roll: -1	F: +682 S: -715	94	99.992	76	99.92
4	20	wire: -38 roll: +1	F: -182 S: +145	47	96.8	28	91.6
5	35	wire: -38 roll: +1	F: -324 S: -288	65	99.4	38	98.2
6	100	wire: -38 roll: +1	F: -756 S: -643	94	99.996	76	99.89

* F = Face side of the fabric **S = Screen side of the fabric

means that the filtration coefficient (μ) had a lower value for the fabrics of higher basis weights.

The charging method in location D is similar to Tech-I, which we will discuss in the next few sections. However, because the collector was made of wire screen, the fibers contacted with the wires were charged better than those on the opening area. This reduced the FE of the fibers in the opening area. Therefore, the overall FE was greatly reduced. The second reason for the lower FE could be that the fibers were still warm or hot when they were subjected to the charges. The charges migrated and disappeared after charging.

The use of two wires with different voltage polarities to charge the fabrics in location E did not show a good surface potential and FE as shown in *Table 5*. The fibers in location E were cooled down and molecular chains were too rigid for the charges to penetrate into the fibers. The wires with the same voltage polarities can not charge the fabrics in location E because the electric field between the wires repel each other and the air is unable to be ionized.

Tech-I can charge, in location E, the lower basis weight fabrics, e.g. 20 g/m^2 and 35 g/m^2, to a moderate surface charge potential and high FE as shown in *Table 6*. The reason why this technology can charge the cold fibers is not fully understood and is still the subject of investigation. However, this technology can only charge the fabrics of high basis weights, e.g. 100g/m^2, to a moderate charge potential and FE, as shown in the same Table. But, this technique can charge the fabric to have a good bipolar property as shown in *Figure 6* for the face side and in *Figure 7* for the screen side. Pure positive charge potential on one side and pure negative charge potential on the other side were observed. The magni-

Figure 6
POSITIVE SURFACE CHARGE POTENTIAL ON THE FACE SIDE OF THE NUMBER 2 FABRIC IN TABLE 6 CHARGED USING TANTRET TECH-1

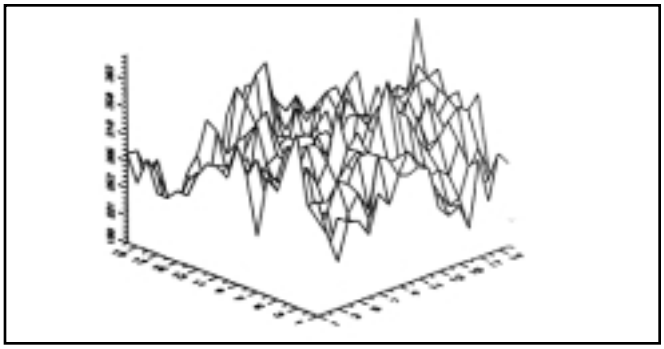

Figure 7
NEGATIVE SURFACE CHARGE POTENTIAL ON THE SCREEN SIDE OF THE FABRIC IN FIGURE 6

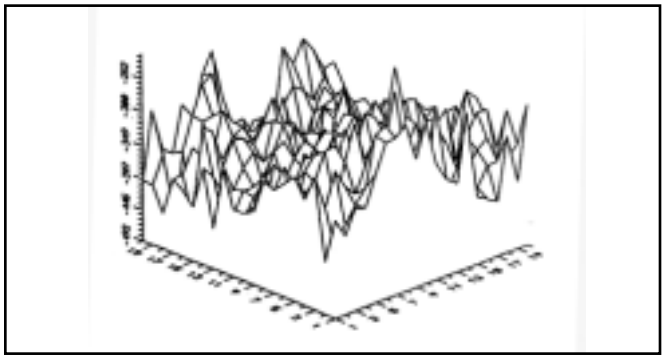

Table 7
SURFACE CHARGE POTENTIAL AND FILTRATION EFFICIENCY OF THE FABRICS CHARGED AT LOCATION E USING TANTRET, TECH-II

Sample Number	Basis Weight (g/m^2)	Charging Voltage (KV)	Surface Charge Potential (V)	Filtration Efficiency (%) Latex control	Latex charged	NaCl control	NaCl charged
1	20	wire: +35 shell: -35	F*: +231 S**: -257	47	88.4	28	73.9
2	35	wire: +35 shell: -35	F: +482 S: -647	65	99.2	38	97.6
3	100	wire: +35 shell: -35	F: +2751 S: -2829	94	99.999	76	99.982
4	20	wire: -35 shell: +35	F: -225 S: +212	47	89.3	28	71.2
5	35	wire: -35 shell: +35	F: -715 S: -688	65	99.6	38	97.9
6	100	wire: -35 shell: +35	F: -2898 S: -2615	94	99.999	76	99.991

* F = Face side of the fabric **S = Screen side of the fabric

tude of the charge potential on both sides was nearly equal.

Tech-II can charge, in location E, the fabrics of different basis weights to a high surface charge potential. However, this technique can only charge the high basis weight fabrics to a high FE and the FE of the fabrics of low basis weight, e.g. $20 g/m^2$ in *Table 7*, charged by Tech-II was much lower than by Tech-I.

Finally, light fabrics had a higher percentage improvement in FE after charging than that of heavy fabrics for all the charging techniques. This does not mean that the FE improve by charging for heavy fabrics is marginal because a small amount percentage increase is critical for high FE media. Therefore, another expression, b-ratio, is also used to denote the filtering ability of a high FE media. It is defined as

$$\beta - ratio = \log(\frac{1}{p}) \text{ ----- } (3)$$

Where p = Penetration.

It can be observed that heavy fabrics had a high improvement in b-ratio after charging, e.g. a light weight fabric of 20 g/m2, Sample 1, Table VI, had an improvement in b-ratio in NaCl testing of 0.965 (from 0.143 to 1.108), while a heavy weight fabric of 100 g/m2, Sample 6, Table VII, had an improvement of 3.4262 in b-ratio (from 0.6198 to 4.046).

Conclusions

The fibers in the MB process could not be charged to a high FE when charged before they were solidified or when they were still hot because the charges migrated and were squeezed out of the fibers. The charges in fibers were randomly distributed either in magnitude or polarity. The fabrics could not be charged after they cooled down in the MB process because the molecular chains were too rigid and closely packed to allow charges to penetrate into the fibers. Tech-I is a good technique to charge the low basis weight fabrics to a high FE, while Tech-II is good to charge the high basis weight fabrics to a high FE. They both charge the fabrics to have bipolar property. However, Tech-II is a good technique to charge both low and high basis weight fabrics to high surface charge potential.

References

1. Wente, Van A. *Industrial Eng. Chem.*, Vol. 48, 1956, P.1342.

2. Hinds, W.C., *Aerosol Technology*, 1982, John Wiley & Sons.

3. Tsai, P.P. and Wadsworth, L.C., "Electrostatic Charging of Meltblown Webs for High-Efficiency Air Filters," *Advances in Filtration and Separation Technology*, Vol. 9, 1995, PP473-491.

4. Smith, P.A., East, G.C., Brown, R.C. and Wake, D., "Generation of Triboelectric charge in Textile Fiber Mixtures and Their Use as Air Filters," *J. Electrostatics*, Vol. 21, 1988, PP81-98.

5. Tsai, P.P., Qin, G.W. and Wadsworth, L.C., "Theory and Techniques of Electrostatic Charging of Meltblown Nonwoven Webs," *TAPPI JOURNAL*, Vol.80, No.7, 1988.

6. Tsai, P.P. and Wadsworth, L.C., "Method and Apparatus for the Electrostatic Charging of a Webs or Films," US Patent 5,401,446, March 28, 1995.

7. Wadsworth, L.C. and Davis, W.T., "Method for Testing Filtration Efficiency," US Patent 4,382,378, May 10, 1983. — ***INJ***

Improving Properties and Processing Performance of Melt-Spun Fibers

By Dale R. Gregory, Polyester Polymers For Fibers, Eastman Chemical Company, Kingsport, Tennessee

Abstract

The properties, yields, and efficiencies achieved in the overall fiber-making process are often governed by the orientation level and by variations in denier and orientation introduced in the extrusion/melt spinning part of that process. Essential to optimization and improved control of these processes is an understanding of the underlying physical phenomena and control of the appropriate variables. This paper builds on 30 years experience and demonstrates what variables need improved control — and why.

Introduction

Melt-spun fibers, including nylons, polyolefins, and polyesters, have been available commercially for over 50 years, and their use continues to expand in various applications, including nonwovens. For most products, processes, and applications, emphasis continues to be placed on increased throughput for a given quality level and/or improved quality for a given throughput. Higher speeds, larger equipment, smaller denier/filament, improved physical properties, improved yields and efficiencies, all at reduced cost, are among those things sought by most fiber producers and fiber users. Considerable progress has been made to achieve these goals, but improvements are still desired and possible. This paper offers some suggestions for further improvements.

Background

The analyses, principles, and measurements discussed in this paper are based on the melt spinning and drawing of poly(ethylene terephthalate) (PET) but are generally applicable to all melt spun fibers. The spinning operation is characterized by the extrusion of molten polymer through small spinneret capillaries into an air quench cabinet where the individual streams attenuate and solidify to form filaments. These filaments are forwarded by means of godet rolls either to be wound onto packages for separate drawing or to be drawn inline. In the drawing operation, as-spun filaments are stretched three to five times their original length, generally at a temperature from 10^{0}C-100^{0}C above the glass transition temperature (Tg) of the polymer, and subsequently heatset to impart dimensional stability. The as-spun fibers have high extensibility, low strength, and low molecular orientation as compared to the drawn fibers. The orientation of the polymer molecules, important to the tensile properties of the final fiber product, occurs in both the spinning and drawing steps of the overall process. Variations in molecular orientation from filament-to-filament and along-each-filament in the as-spun yarn plays a crucial role in the properties, processibility, efficiencies, and yields of the final fiber product as we shall discuss.

Other authors have published several papers pertinent to this discussion in recent years [1-13]. George showed [1] that the stress at the freeze point (usually taken as Tg) in the moving threadline during melt spinning correlates well with the spun yarn birefringence (measure of molecular orientation) which in turn correlates well with spun yarn tenacity, % elongation, and initial modulus. George also mentioned [1] that, "while the total flow is carefully metered by the melt pump, the flow to individual capillaries is regulated by an hydraulic split, which points up the need for precise tolerances on the hole dimensions." Dutta and Nadkarni verified [2] the findings of George for spinning speeds below 3,000 m/min. and also found that "extrusion temperature, melt intrinsic viscosity, feed rate, and take-up velocity are the key variables for PET melt spinning, as they strongly affect the freeze line location and the as-spun orientation." Dutta and Nadkarni also cautioned [2] that careful control of these key variables is essential for good processibility and fiber properties: "The uniformity of the fiber quality would be influenced by the fiber-line stress distribution in the multifilament bundle." Shenoy and Nadkarni completed a case study [3], which indicated "that it may be feasible to improve spinning productivity without affecting fiberline processibility only by appro-

priate changes in the melt spinning parameters." Dutta in the first [4] of three additional papers [4-6] showed that "the complex interactions between the filament bundle geometry and the quench conditions are likely to play a critical role in controlling spun fiber properties and their variability." He also confirmed [5] using a computer simulation approach "that the quench conditions seen by the filaments within a bundle are not identical, but differ for different rows of filaments." Dutta also pointed out [6] that "for commercial operations, not only are the average properties of the fiber bundle important in downstream operations like drawing, heat setting, texturizing, etc., but the extent of variability in each fiber property is also equally critical." King pointed out [7] that not only spun properties are important but also "the definition of drawing conditions becomes a critical element when the goal of the investigator is to optimize a drawn product, given changes in both spinning and drawing." King [7], Perez [8], and Vassilatos et al. [9] have also shown that physical property development for PET is a unique function of molecular orientation regardless of whether the orientation is experienced in spinning or cold drawing. The four other papers cited [10-13] are of general interest.

Discussion

Our work of the past 30-plus years [14-21] agrees in general with the findings and conclusions of the work discussed above [1-9]. Two topics which should be considered in addition to those highlighted above are the known, measured thermal sensitivity of molten polyesters [17-19] including PET and the strong power function (5.1) of IV (inherent or intrinsic viscosity) on melt viscosity [14-16]. PET degrades (IV decreases) when it is molten in the spinning machine (even for short residence times) significantly affecting the melt viscosity nonuniformly and thereby the flow distribution through the spinneret. The mass (denier) distribution is thereby broadened, as is the companion orientation distribution in the as-spun filaments. These nonuniformities originating from these sources in the spinning step and nonuniform quenching conditions together have negative consequences in subsequent processing performance and in final product properties. Let's see how.

Consider the flow of molten PET through a mulifilament spinneret (*Figure 1)*. Polymer pellets have been melted in the plasticating extruder, and the melt has been metered through spinpack filters to the upstream side of the multicapillary spinneret. The total flow rate of the melt delivered to the spinneret by the close-tolerance gear pump, operating within its design capabilities and inverter driven at constant speed, is essentially constant. Therefore, the filament-to-filament and along-a-filament denier distribution known to exist [1-6, 20, 21, 24] in all multifilament PET yarns must arise downstream of the pump. Since the flow rate from the pump is constant, the total flow rate to and through the spinneret (all capillaries) is constant. The division of that flow to each capillary, which determines the overall individual filament denier (g/9000 meters), need not be equal (mentioned by George [1]), as can be shown from the following equation:

Figure 1
SPINNERET ASSEMBLY

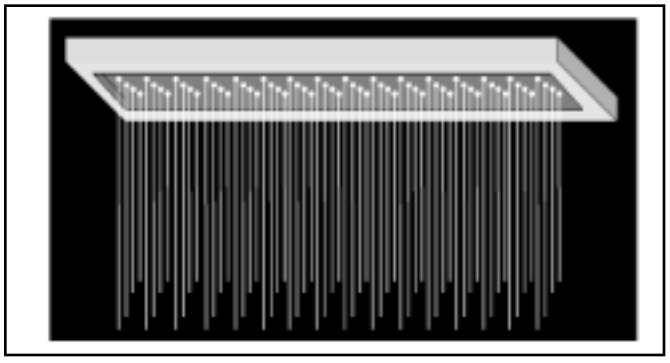

$$Q = \frac{\pi R^4 \Delta P}{8 \eta_0 L} \qquad (1)$$

Equation 1 relates the volumetric flow rate, Q, through each capillary to the forces causing that flow for Newtonian fluids and round cross-section capillaries. Similar equations apply to flow through nonround cross sections. Molten PET has been shown [14-15] to be Newtonian in behavior for shear stresses < 14 psi, a condition normally met in typical melt spinning below 3,000 m/min. For flow conditions with shear stresses > 14 psi, an equation describing the shear sensitivity of molten PET was also determined [14-15] and can be used for those conditions.

Let's examine each term in Equation 1 for its influence on filament-to-filament denier distribution. The pressure in the distribution space between the bottom of the filter medium and the back of the spinneret is constant if the space is sufficiently wide (no radial or θ gradients). The pressure drop, ΔP, across each capillary for all capillaries is therefore the same and does not contribute to the denier distribution. The variations in filament-to-filament denier (Q for each capillary) must therefore result from variations in R, L, and η_o (melt viscosity). The capillary dimensions R and L (round capillaries) are predetermined in the manufacture of the spinneret, and their contributions to filament-to-filament denier variations, although important [1], are largely fixed and can be calculated based on measurements of capillary dimensions [20-21]. Note the 4th power influence of capillary radius, R. Wear and tear on spinneret capillaries during multiple uses in the production process can influence denier distributions, too [20-21]. Control of capillary dimensions is a necessary but not a sufficient condition for control of filament-to-filament denier.

Note also from Equation 1 that the flow through each capillary depends inversely on the melt viscosity of the polymer feeding each capillary. If the melt viscosity of the polymer in the space just above the spinneret varies from location to location (and it does because of residence time differences, temperature gradients, and resulting variations from thermal

degradation), the flow from capillary-to-capillary must be different because of this source, too. Melt viscosity for PET is given by [14-15]:

$$\eta_0 = 0.098e^{\left(\frac{6800}{T}\right)}(IV)^{5.1} \qquad (2)$$

where: η_0 = Newtonian melt viscosity, poise
T = absolute temperature, °k
IV = inherent viscosity

Note from Equation 2 that melt viscosity of PET is a strong power function (5.1 power) of IV and an exponential function of temperature. For example, for PET of 0.60 IV, a 0.01 change in IV accounts for the same change in melt viscosity as a 4°C (7.2°F) change in melt temperature. IV and temperature differences from location-to-location in the spinpack assembly will, therefore, affect the filament-to-filament denier distribution because of their effects on melt viscosity. In fact, because of the nature of the flow (laminar) and flow distribution in most melt spinning systems, both IV gradients (largely from residence time differences, temperature differences, and thermal degradation) and temperature gradients exist, and their influence on denier and orientation distributions follows the gradients.

Thermal, hydrolytic, and oxidative degradation all occur during melt processing of PET and often are not measured, accommodated, or reduced. Many of the problems encountered in the extrusion, melt spinning, and processing of PET fibers are caused or influenced by one or more of these degradation processes. Understanding of the degradation behaviors of molten PET will help in devising ways to reduce their detrimental influences.

Thermal degradation occurs whenever PET is molten, even in the polymerization vessel where the reaction is processing. The mechanisms in the polymerization vessel and in direct spinning (melt spinning directly from the final polymer reactor without pelletizing and remelting) and that in remelting from pellets, e.g., in plasticating extrusion, are apparently different by at least a factor of 10 (perhaps more) as shown by Zemblowski and Torzecki [22] and attributed by them to a temperature dependent induction time before onset of degradation. Polyesters including PET degrade thermally mainly by random chain scission [17-18]. In chain scission, chemical bonds are broken at random within the polymer molecules. Each scission creates two shorter molecules and lowers the average molecular weight (IV) of the polymer. For PET, the equation for thermal degradation during remelting and processing is [17, 18, 20]:

$$\left(\frac{1}{IV_t}\right)^{1.47} = \left(\frac{1}{IV_o}\right)^{1.47} + \left\{e^{\left[\frac{26.9 - 17{,}080}{T}\right]}\right\}t \qquad (3)$$

where: IV_t = IV of polymer at time t
IV_o = IV of supply polymer (t = o)
t = residence time in the melt, minutes
T = absolute temperature, °k (°C + 273°)

Equation 3 was derived theoretically but verified experimentally, and it describes PET thermal degradation during remelting from pellets very well. A typical PET melt spinning process might use a supply polymer with IV_o = 0.60, an average melt temperature of 290°C, and an average melt residence time of 5 minutes. The resulting as-spun fiber IV_t from Equation (3) would be 0.57. Reduction in residence time to 3 minutes at 290°C would yield a fiber IV_t of 0.585 (0.015 IV units higher, equivalent in effect to lowering melt temperature by 6°C at 5 minutes residence time). Remember the 5.1 power function of IV on melt viscosity.

The reaction of water present in the PET supply polymer to the extruder is virtually instantaneous in comparison with the thermal degradation during extrusion [18-20]. The water present reacts so rapidly, it merely adjusts the starting IV. The following equation was developed for the hydrolytic degradation of PET [18-20]:

$$IV_H = \frac{IV_o}{\left[1 + 21.9(x)(IV_o)^{1.47}\right]^{0.68}} \qquad (4)$$

where: IV_H = inherent viscosity after reaction with water
IV_o = inherent viscosity of supply polymer
X = weight % of water in supply polymer

Figure 2 (based on Equation 4) shows the IV breakdown of PET as a function of moisture content. Note from Equation 4 and *Figure 2* that hydrolysis of PET is a function of supply polymer IV_o as well as the moisture content itself, i.e., ΔIV is greater for a higher IV_o at a given moisture content.

Most of the water present in PET polymer as it feeds an

Figure 2
MELT PROCESSING OF PET POLYMER — BREAKDOWN OF PET AS A FUNCTION OF MOISTURE CONTENT

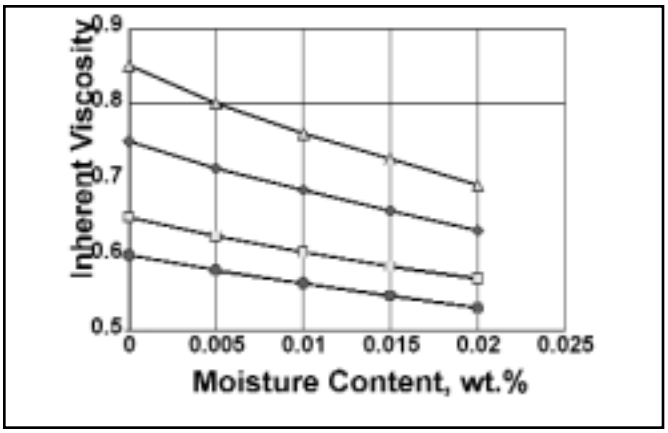

Figure 3
SUMMARY OF DRYING

1. PET is hygroscopic—it readily takes up moisture and retains moisture upon exposure, e.g., moisture in transport gas.
2. PET must be dried and kept dry to avoid hydrolysis during melt processing; it will readily and quickly pick up moisture from air/nitrogen during transport/storage.
3. Transport/storage systems for dried PET need to be sealed against ingress of moist air, thus re-contaminating the polymer.
4. In melt extruders, moisture hydrolyzes PET pellets instantaneously and quantitiatively up to about 0.02 weight %, and above that level the extruder acts as a dryer.
5. Dependent on temperature, residence time and polymer IV, thermal breakdown, though slower than hydrolysis, continues as long as the PET is molten.
6. A 0.05 decrease in IV results in melt viscosity decrease of ~ 50% such that every 0.01 decrease in IV has the effect on melt viscosity as an increase in temperature of 4^{0}C.

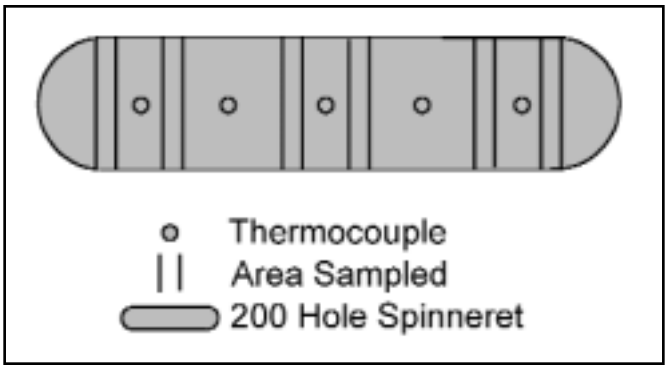

Figure 4
MODIFIED SPINNERET SHOWING AREAS SAMPLED AND THERMOCOUPLE LOCATION

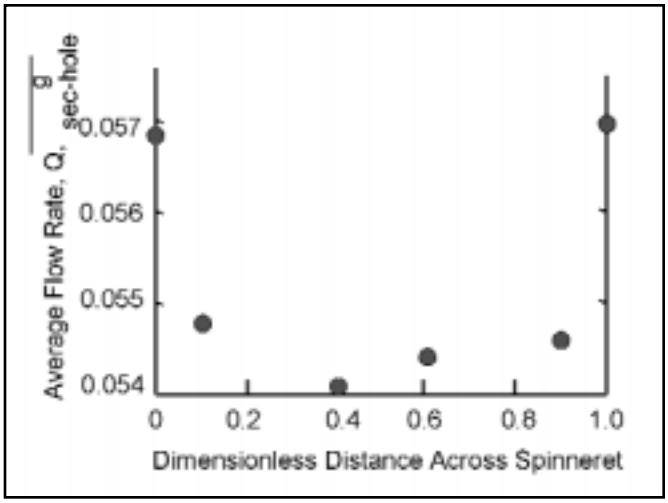

Figure 5
FLOW PROFILE FOR ONE SPINNERET

extruder will react with polymer resulting in a reduced IV (and melt viscosity). Some of the water, however, will vaporize and leave the extruder via the feed throat. For PET, water concentrations above about 0.02 weight % will vaporize and not react in a plasticating extruder [18, 20]. Normally, one wants the fiber IV to be uniform and as nearly equal to the polymer IV as possible, otherwise one has wasted money, time, and effort in producing the polymer IV supplied. Therefore, it is recommended that PET be dried prior to extrusion. From a quality standpoint, uniform drying is more important then is level of drying because nonuniform drying could lead to nonuniform IV and flow distribution differences associated with localized differences in melt viscosity. Note that dry PET is highly hygroscopic, and care should be exercised that, once dry, it does not come into contact with moisture again, including even nondry air. It will pick up moisture if it does. *Figure 3* gives Rules of Thumb concerning the drying of PET.

Under certain conditions, oxygen reacts with PET to form a crosslinked species, often called gels, which is sufficiently different in properties from those of the bulk polymer that broken filaments result in spinning and drawing [20]. These crosslinked species may arise either in polymerization from an air leak or in melt spinning from presence of air in the supply polymer. The crosslinked species is usually deformable and can be reduced in size and thereby in detrimental behavior by proper shearing in the spinpack during the melt spinning operation [21]. However, the best way to deal with it is not to allow it to form; seal the reactors against air leaks and nitrogen purge the extruder feed throat.

We measured substantial gradients in IV, melt flow rate (denier)/capillary, and temperature in production spinpacks [20]. Average flow rate per capillary and fiber IVs were determined across the spinneret face on 11 production spinning positions (*Figure 4)*. Temperature profiles and capillary dimensions were also measured on the same positions. Flow rate differences ranging from 3% to 27% with an average of 11% were found to exist between center and end capillaries of the 11 spinning positions sampled (*Figure 5)*. IV distribution (probably from residence time distribution of the flowing melt and differences in thermal degradation) was found to be the major cause of flow rate (denier) difference (*Figure 6)*. The temperature distribution was such that its effect on flow rate was opposite to that of the IV distribution (*Figure 7)*. Variations in capillary dimensions in this system accounted for only about 10% to 20% of the variation measured in the delivery rate per capillary and therefore the average denier/filament. Significant improvements in multifilament spun denier uniformity from filament-to-filament can be accomplished by reducing IV and temperature gradients

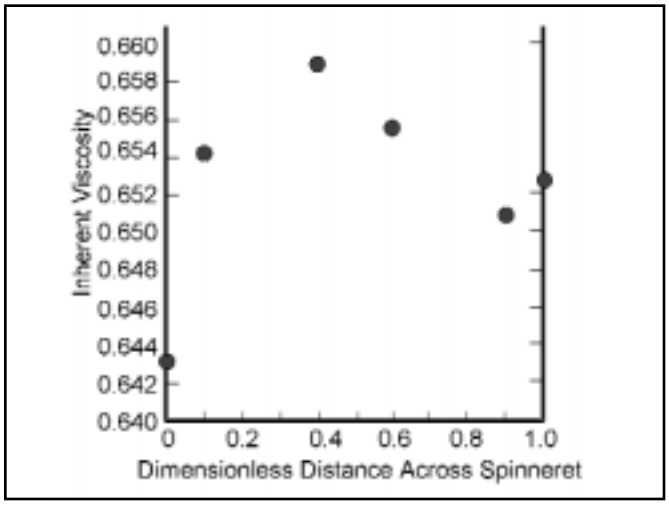

Figure 6
INHERENT VISCOSITY PROFILE FOR ONE SPINNERET

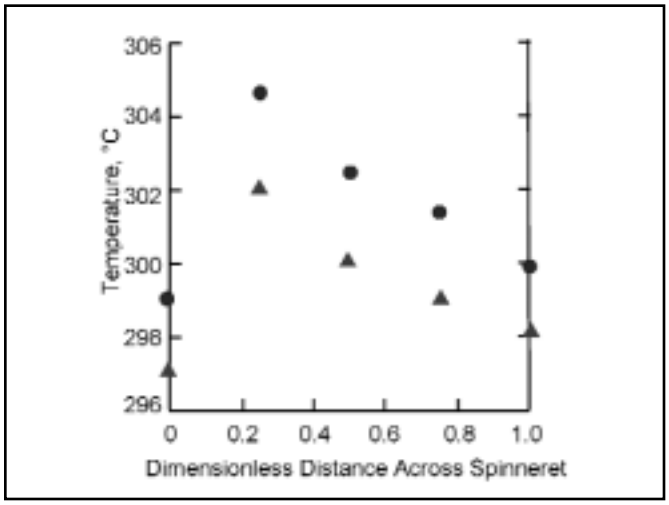

Figure 7
TEMPERATURE PROFILE ACROSS SPINNERET FACE

upstream of the spinneret as well as improving hole geometry uniformity. Techniques for accomplishing these improvements are system and polymer dependent. Relative contributions of the various contributors to the denier nonuniformity need to be quantified for the system and polymer being used, and remedial actions need to be designed and implemented based on these contributions. Inline mixers just upstream of the spinpack, flow distribution devices in the distribution space just above the spinneret, and redesigned spinpacks and heaters are some techniques which have been used successfully [20].

Let's now consider along-a-filament denier distribution. What happens to the filaments after they emerge from the capillaries? In steady state operation, the total mass of fiber in the spin column (all filaments in the threadline) at any time is constant [determined by the gear pump (size and speed), the speed of the first godet roll (nonslip condition), and the length of the spin column (residence time)]. The same is true for each filament even though the mass (denier) in the column from filament-to-filament will be different, as explained above. When each filament emerges from each capillary, it is molten and easily responds to the forces imposed on it (transverse as well as axial). The filaments attenuate and cool (not necessarily uniformly and at the same rate) and solidify (not necessarily at the same time and place in the spin column). For a typical PET melt spinning process below 3000 m/min, filaments are usually at Tg within 1 meter below the spinneret face on the average, but with variation in freeze point location from filament-to-filament [20-24]. Orientation of the molecules achieved in each as-spun filament will therefore vary from filament-to-filament, thus potentially leading to processing problems such as broken filaments, roll wraps, and filament loops often with reduced yields, reduced spinning and processing speeds, and/or inadequate tensile properties.

The variation in forces imposed when the filaments are above Tg, normally from variations in quench air conditions (turbulence [20], multiple rows of filaments [4], etc.), lead to along-a-filament denier variations in addition to filament-to-filament variations already introduced when the polymer passed through the spinneret. Each filament distributes its mass in the spin column in response to the forces acting on it, primarily in the upper part of the spin column. Multifilament fibers usually have both types of denier variations (and coincident molecular orientation variations), but their origins and remedies are usually different, as we have discussed.

We measured filament diameter and birefringence of several as-spun filaments from each multifilament threadline from a 16-position, production sized spinning machine. Birefringence of round cross section fibers is a measure of molecular orientation imposed on the fiber [25]. The average filament birefringence as a function of the average filament diameter for as-spun yarn from each spinning position is presented in *Figure 8*. A smooth curve fits the data well for a range in average filament diameter from 21 to 27.3 microns and a range in birefringence from 0.0069 to 0.0109. A single point instead of a line would have resulted if the yarn had been completely uniform in size and molecular orientation. Note also that the data points of *Figure 8* are averages of 20 values and not the individual values. *Figure 9* shows the relationship between diameter and birefringence for the 20 individual measurements taken 2 1/2 inches apart along one typical as-spun filament. Note the regular variation in each and the "mirror image" of diameter and birefringence; as the filament first gets smaller and then larger along its length, the molecular orientation first increases and then decreases in tandem. This behavior existed in all filaments measured regardless of their average sizes. Ziabicki and Kadzierska had shown [26] this inverse effect of diameter and birefringence in some of their early work.

What are the implications of *Figure 8* and *Figure 9*? As the individual filaments of a multifilament threadline are formed and the molecules are oriented simultaneously in the spin column, the smaller diameter fibers (overall from filament-to-filament and along each filament) have higher as-spun orien-

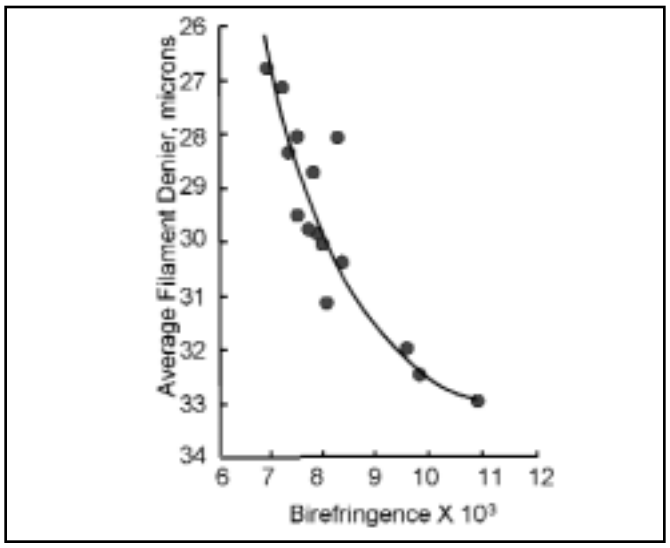

Figure 8
AVERAGE FILAMENT DIAMETER VS. AVERAGE FILAMENT BIREFRINGENCE FOR EACH POSITION ON SPINNING MACHINE

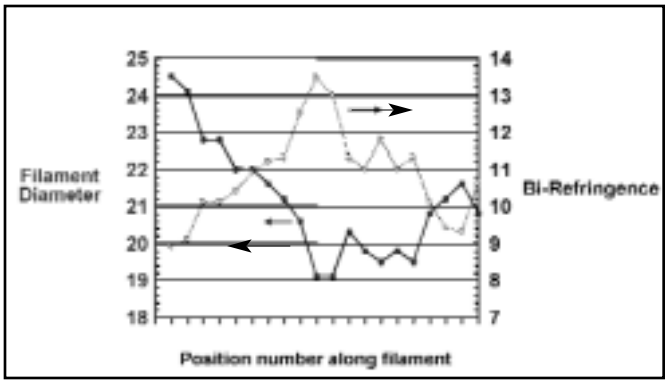

Figure 9
PET SINGLE FILAMENT ANALYSIS — 20 SUCCESSIVE POINTS 2.5 INCHES APART

tation (birefringence) than the larger ones. In a typical fiber process, the multifilament as-spun yarn is then drawn (extended) 3-5 times its original length to orient the molecules further and achieve its final tensile properties (tenacity, % elongation, modulus, etc. usually considered and reported as averages perhaps with some measures of variation). Remember, King and others [7-9] showed that physical property development for PET is a unique function of molecular orientation regardless of whether the orientation is achieved in spinning or drawing. King also showed [5] that the breaking draw ratio and the natural draw ratio of as-spun PET are strong functions of birefringence, particularly from 0.001 to 0.015 (e.g., the breaking draw ratio for 0.006 birefringence is 5 and for 0.011 birefringence is 3.5 from *Figure 2* of his work).

Variations in denier, denier/filament, and orientation/filament, achieved in the drawn yarn, result primarily from the variations introduced in the as-spun yarn. This statement is true because the filaments in the multifilament as-spun yarn are extended to an identical extent (draw ratio of the drawing step without slippage) essentially in parallel. The variations in as-spun orientation from filament-to-filament and along a filament can be large enough [20-21] such that the smaller, more highly oriented, filaments will break often wrapping a roll in drawing as the process is set up or adjusted to achieve the desired average drawn yarn properties. Gregory, Phillips, and Wang made an analysis of roll wrap formation in our earlier paper [28]. The overall ranges of measured birefringence and denier/filament of the production as-spun yarn shown in *Figure 8* were from 0.0069 to 0.0109 and 2.2 to 9.9 (average of 6.3), respectively. This as-spun yarn was drawn in a production staple process at a 4.2 draw ratio to a final average drawn denier/filament of 1.5. Note that the 4.2 production draw ratio in use exceeded the breaking draw ratio for the smaller, more highly oriented as-spun filaments, i.e., those filaments with birefringence greater than 0.008 (from King's work [5]). These smaller filaments would be expected to break in drawing, and the presence of "harsh" fibers in the final product suggested strongly that in fact they did. Another indication of broken filaments was measured. If the small as-spun filaments (2.2 denier/filament) had survived drawing at a draw ratio of 4.2 without breaking, their drawn denier/filament would have been 0.5. No filaments smaller than 0.9 denier/filament were found in the drawn yarn suggesting that as-spun filaments smaller than 3.8 denier/filament (0.9 x 4.2 draw ratio) had indeed broken.

But what about the larger filaments in the distribution? As mentioned above, the largest denier/filament fiber in the production as-spun yarn of *Figure 8* was 9.9. It also had the lowest average orientation. When drawn with all the other fibers using the 4.2 draw ratio, its drawn denier/filament was about 2.4, and it still had the lowest average orientation. When heat-set, this large, less-oriented filament would not shrink as much as the more highly oriented filaments. It would therefore be longer and might protrude [27] from the threadline forming "filament loops," more of a problem in filament yarns than in staple yarns, but a problem nevertheless.

A word of caution is in order. One must be careful in measurements of denier and denier variations. Remember that denier is defined as the weight in grams of 9,000 meters of fiber; no one I know uses 9,000 meters or more, particularly of individual filaments; however, one often assumes (often implicitly) that a filament with a round cross section is a cylinder and often of great length. Our measurements discussed here [20, 21, 24] have shown that this assumption is not true because of variations (often short term) in diameter along each filament. If short lengths of individual fibers are used (cross section diameter or area measurements suffer the most), the measurement includes both filament-to-filament and along-a-filament contributions. To avoid this confounding for filament-to-filament measurements, one must use fairly long lengths of fibers, at least as long as the freezeline distance (distance from the spinneret face to where the filament attenuation stops). Measurements made on the same sample of multifilament yarn showed [21] that as length of sample increased, the measured filament-to-filament "denier" varia-

tion decreased until it became essentially constant. At that point, we were confident that we were measuring the true filament-to-filament variation independent of along-a-filament contributions; we in essence "smoothed out" the along-a-filament variations.

Many production melt spinning/drawing processes are set up either one or the other following objectives: (1) to maximize throughput (productivity) at a given set of properties, quality, and yield (acceptable level of broken filaments, roll wraps, and filament loops usually in drawn yarn); (2) to improve the properties (e.g., higher tenacity), quality, and yield (reduced level of broken filaments, roll wraps, and filament loops) at a given acceptable throughput. Results discussed here [1-9, 14-23] have shown that improved uniformities of denier/filament and orientation/filament, particularly in the as-spun yarn, are essential to the achievement of either objective.

Summary

For PET, improvements in properties, throughputs, and quality of drawn fiber products will result from improvements made in the uniformity of as-spun fiber properties, particularly denier/filament and the attendant orientation/filament. Reduced melt viscosity variations in the spinpack from reduced IV, residence time, and temperature gradients will yield reduced denier and orientation variations from filament-to-filament in addition to those from improved capillary uniformity. Improved quench system and quench airflow designs will reduce along-a-filament denier and orientation variations. Both improvements are often needed.

The analyses, principles, and measurements discussed in this paper, although specific to round cross section PET, are generally applicable to other melt spun fibers and other cross sections.

Acknowledgements

Thanks to C. V. McDonnell, who first demonstrated to me the importance of nonuniformities in as-spun yarn and techniques to evaluate and reduce those nonuniformities. Thanks also to Fred C. Wampler, C. B. Wang, W. W. Rowell, W. A. Haile, L. R. Dean, James O. Casey, Frank O. Harris, Bobby M. Phillips, A. K. "Gus" Meyer, W. M. McSpadden, and E. E. Oliver for sharing work and discussions over the past 30+ years. A special thanks to the Polymers-For-Fibers Team at Eastman Chemical Company for making the past two years a most enjoyable experience.

References

1. H. H. George, *Polym. Eng. And Sci.*, V22, n5, 292-299 (1982).

2. A. Dutta and V. M. Nadkarni, *Text. Res. J.*, V54, 35-42 (1984).

3. A. V. Shenoy and V. M. Nadkarni, *Text. Res. J.*, V54, 778-783 (1984).

4. A. Dutta, *Text. Res. J.*, V57, 13-19 (1987).

5. A. Dutta, *Polym. Eng. and Sci.*, V27, n14, 1050-1058 (1987).

6. A. Dutta, *Text. Res. J.*, V59, 411-415 (1989).

7. C. M. King, *J. Appl. Polym. Sci.*, Appl. Polym. Symp. 47, 171-181 (1991).

8. G. Perez, in High-Speed Fiber Spinning, Chap. 12, Wiley-Interscience, New York, 1985.

9. G. Vassilatos et al., in High-Speed Fiber Spinning, Chap. 14, Wiley-Interscience, NY, 1985.

10. H. Brunig, R. Bayreuther, and H. Hofman, *IFJ*, 104-107 (April, 1999).

11. K. Riggert, *Mod. Text.*, 63-65 (July, 1974).

12. L. C. T. Lin and J. Hauenstein, *J. Appl. Polym. Sci.*, V18, 3509-3521 (1974).

13. A. Ziabicki, L. Jarecki, and A.Wasiak, *Comp. and Theor. Polym. Sci.*, V8, n 1/2, 143-157 (1998).

14. D. R. Gregory and M. T. Watson, *J. Polym. Sci., Pt. C.*, n3, 399-406 (1970).

15. D. R. Gregory, *J. Appl. Polym. Sci.*, V16, 1479-1487 (1972).

16. D. R. Gregory, *Trans. Soc. Rheol.*, V17, n1, 191-195 (1973).

17. D. R. Gregory and M. T. Watson, *Polym. Engr. and Sci.*, V12, n6, 454-458 (1972).

18. F. C. Wampler and D. R. Gregory, *J. Appl. Polym. Sci.* V16, 3253-3263 (1972).

19. D. R. Gregory and F. C. Wampler, *Polym. Engr. and Sci.*, V25, n6, 362-366 (1985).

20. F. C. Wampler and D. R. Gregory, unpublished experimental work, 1966-1972.

21. D. R. Gregory, unpublished work, 1968.

22. Z. Kemblowski and J. Torzecki, *Polym. Engr. and Sci.*, V22, n3, 141-146 (1982).

23. D. L. Nealy, unpublished work, 1970.

24. D. R. Gregory et al., unpublished work, 1999.

25. W. E. Morton and J. W. S. Hearle, *Physical Properties of Textile Fibers*, pp. 524-545, Butterworth & Co., Ltd., London, 1962.

26. A. Ziabicki and K. Kedzierska, *J. Appl. Polym. Sci.*, V6, n19, 111-119 (1962).

27. C. V. McDonnell and D. R. Gregory, unpublished work, 1961-1962.

28. D. R. Gregory, B. M. Phillips, and C. B. Wang, *Text. Res. J.*, V54, n12, 793-802 (1984). ***— INJ***

A Study of the Airflow and Fibre Dynamics in the Transport Chamber of a Sifting Air-laying System: Part 2 — Fibre Dynamics

By A. Pourmohammadi and S.J. Russell, Nonwovens Research Group, School of Textile Industries; R. Bradean, D.B. Ingham and X. Wen, Centre for CFD, University of Leeds, UK

Abstract

In Part 1 of this paper *(International Nonwovens Journal, Summer 2000),* the airflow characteristics in the transport chamber of a sifting air-laying system of the Kroyer type [US patent 4,144,619] was reported. In Part 2, the fibre dynamics in the transport chamber of the machine are investigated. These are of major practical importance because they influence the process of web formation. High-speed photography was used to observe fibres in flight and their deposition onto the conveyor belt during web formation using fixed machine conditions. It was established that fibres move intensively in three dimensions at the top of the chamber and as they travel towards the landing area their motion becomes more uniform. Fibre landing behaviour was studied by analysing photographic images. Using standard machine settings, it was established that about 38% of fibres landed end-on before falling down flat onto the conveyor belt (Hit-Fall configuration) and about 30% of fibres landed flat (along their full length) but bounced before coming to rest on the conveyor belt (Hit and Bounce configuration). Fibres were deformed when passing through the top grid, causing permanent deformation that was evident in the fibres landing on the conveyor belt.

Introduction

The utilisation of high-speed photography as a means of visualising fibre flow in textile processes is well established. Lawrence and Chen [1988] used high-speed cine photography in their study of the removal of fibres from the opening roller and their passage through the transport channel during rotor spinning. Allen [1991] used the same technique to investigate the fibre flow in friction spinning. Lawrence and Jiang [1996] employed high-speed photography to observe fibres in flight and their deposition onto the forming end of a yarn in the disc-spinning process. High-speed photographic observations of fibres leaving metallic clothed cylinder in the transport chamber of a Fehrer K12-type air-laying machine have also been reported [Pourmohammadi 1998]. In the present research, high-speed photography was used to elucidate fundamental aspects of fibre motion in the transport chamber and fibre deposition onto the conveyor belt during a sifting air-laying process. Previously, little work of this type has been reported in the public domain.

Experimental procedure

To facilitate photography, it was necessary to construct a glass-viewing window at one side of the transport chamber. Initially, it was noticed that during air laying, fibres became electrostatically charged and adhered to the window, causing poor viewing conditions. A conductive-coated glass was therefore fitted to the viewing window to discharge the fibres and release them from the surface. In order to capture the fibres in such a large transport chamber (8 X 45 X 50 cm HWL) a matt black scaled diffuser plate was placed in the chamber to confine the photographic area. After extensive off-site testing with different optical arrangements, it was found that a viewing area of 17 X 19 mm, using a TV lens with 20 times magnification, and a camera-to-plate setting distance of 120 mm provided an acceptable image of the fibres in the transport chamber.

Preliminary studies in the transport chamber were undertaken using both a high-speed cine camera and a high-speed

CCD video camera. Although the high-speed cine camera offers a higher framing rate and image resolution, high-speed video provides the advantage of ease of use, live picture set-up, reusable recording media and most importantly immediate playback capabilities. Therefore, for most of the experimental work, a Kodak Ektapro HS (CCD video camera), Model 4540 was used. This system is capable of recording up to 4500 full frames per second (ffps) and 40,500 partial frames per second (pfps) with a resolution of 256 X 256 pixels, which is equivalent to 3000 ISO. The camera speed was set to 4500 ffps and a TV lens with the smallest aperture (to obtain the maximum depth of field) was used.

In this particular study, short (5 mm length), uncrimped, 28 dtex viscose rayon fibres were utilised. These fibres were obtained from a commercial fibre producer and while being coarser than typically used by the pulp industry, they were used as part of a wider study of this air-laying process concerned with the recycling of short fibre waste. The air/fibre mixture used in this experiment was $2.1m^3$ of air/gr. of fibres. The machine settings used were summarised in Part 1 of this paper.

Experimental Results

As explained in the previous section, the optimum viewing area was 17¥19 mm and therefore, in order to visualise the whole chamber height (of 80 mm), it was necessary to establish four sections and photography was carried out separately in each section. About two hours of film footage was recorded. The following results are obtained from viewing all the film footage and some typical fibre images in the transport chamber are shown in *Figures 1-4*. (For reference, see Part 1, Figure 1: Lower Chamber, *International Nonwovens Journal*, Summer 2000.)

Summary of Observations in the Transport Chamber

Section I: In *Figure 1*, the top grid through which fibres pass from the fibre dispersing zone to the transport chamber is shown at the top of the image. It was observed that a minority of fibres (about 23%) were slightly deformed by passage through the grid, causing permanent curvature, but most were not deformed and remained rod-like (*Figure 1*). Fibres were frequently retarded during their passage through the grid. The motion of fibres in this section was chaotic with intensive rotation and translation in all three dimensions (X, Y, Z). As fibres travelled further down through the chamber their motion became more uniform and the velocity of fibres generally increased, reflecting the trends in the airflow velocity results presented in Part 1 of the paper.

Section II: *Figure 2* shows fibres in the second section of the transport chamber. Hooked and straight fibres are clearly evident. As mentioned above, the hooked configuration was usually created as fibres passed through the top grid. Interestingly, the shape configuration of fibres did not appear to be affected by airflow conditions in the transport chamber. It is important to mention that finer fibres may have shown different deformation behaviour as they pass through the top grid. It is likely that fibre configuration will depend on fibre rigidity and fibre length. This will be researched further.

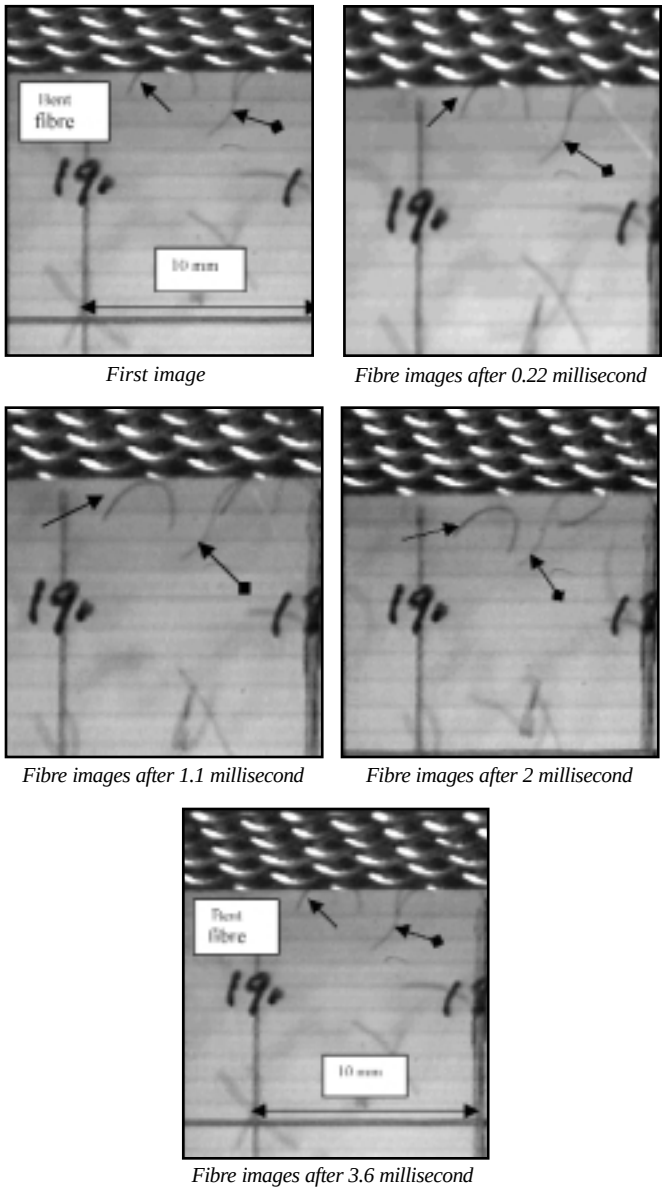

First image | *Fibre images after 0.22 millisecond*

Fibre images after 1.1 millisecond | *Fibre images after 2 millisecond*

Fibre images after 3.6 millisecond

Figure 1
SEQUENTIAL FRAMES SHOWING FIBRES RELEASING FROM THE TOP GRID

Note: The arrows highlight individual fibres that may be tracked in the subsequent frames. Notice that the curved fibre (deformed during passage through the top grid) does not change configuration when released from the top grid. Some fibres are also temporarily retained by the grid. The distance from the exit of the transport chamber is 190 mm.

Section III: In the third section of the transport chamber, fibres were subject to less rotation, reflecting a less turbulent airflow (the airflow was known to be more uniform in this region from results obtained in Part 1 of the paper). *Figure 3* shows examples of fibres travelling through the third section and both bent and straight fibre configurations are again apparent. In general, the shape configurations of fibres moving from the top to the bottom of the transport chamber did not change. Despite rotation and interaction of fibres with

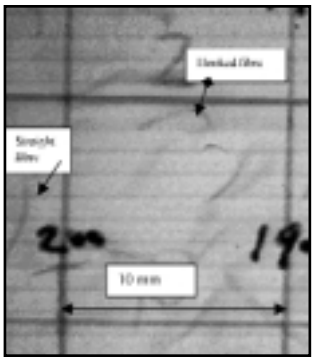

First image

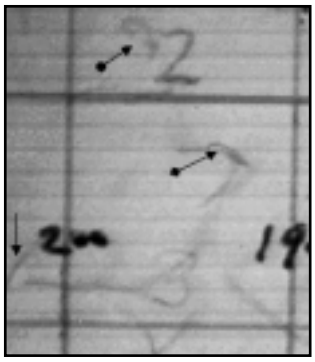

Fibre images after 1.3 millisecond

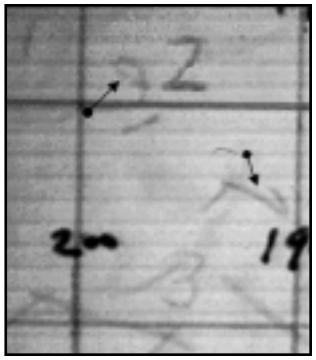

Fibre images after 2.7 millisecond

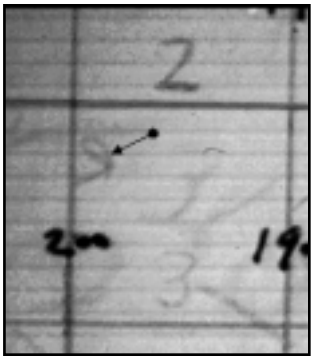

Fibre images after 5.8 millisecond

Figure 2
FIBRES IN THE SECOND SECTION OF THE CHAMBER (HOOKED AND STRAIGHT FIBRES ARE VISIBLE)

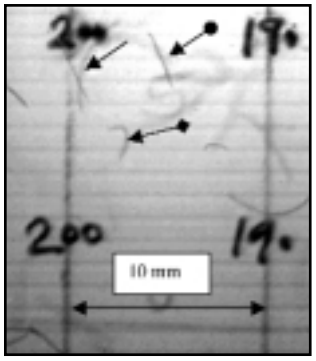

First image

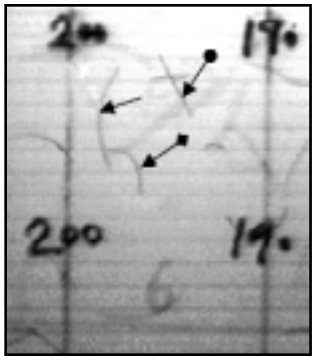

Fibre images after 2.2 millisecond

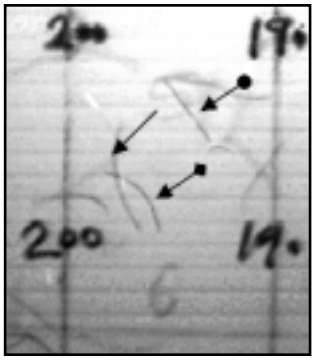

Fibre images after 4.4 millisecond

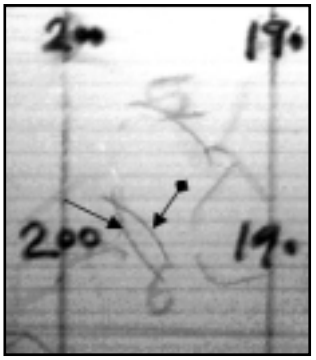

Fibre images after 6.7 millisecond

Figure 3
FIBRES IN THE THIRD SECTION OF THE CHAMBER

Note: In this sequence, fibres can be tracked through section three of the transport chamber. It is evident that interference among individual fibres occurs, which can lead to the formation of small bunches of fibres that may separate or combine further during passage through the chamber.

others during transport to the conveyor belt, analysis of the film footage indicated that most fibres (about 78%) remained rod-like and straight as they passed through the transport chamber.

Section IV: *Figure 4* shows the landing area. This is arguably the most critical region of the transport chamber because it is here that the web is formed. In this area, incoming fibres are decelerated and either hit the empty conveyor belt or land on previously laid fibres. It was observed that if fibres land on an empty belt, depending on the approach angle, they tended to bounce before coming to rest. The ends of some incoming fibres also became trapped in the holes of the conveyor belt mesh and therefore retain their incoming approach angle. When incoming fibres were deposited on an existing fibre layer, their approach configuration tended to be retained and the fibres were incorporated into the forming web structure with a similar orientation.

Fibre Landing Behaviour on the Conveyor Belt

Using typical machine settings the manner of fibre deposition on the conveyor belt was revealed. These conditions were defined in Part 1, Section 2.

In order to characterise the modes of fibre deposition on the conveyor belt a classification system based on extensive photographic evidence was introduced, as indicated in *Figures 5a and 5b*. These photographic images of fibres were taken in the plane X = 120 mm and along the length of the chamber (Y = 160-350 mm). *Figures 5a and 5b* show sequential images of fibre deposition in each class. Based on the classification of 600 randomly selected individual fibres landing on an empty belt, a frequency distribution was constructed to characterise the landing behaviour of fibres during web formation (*Figure 6)*. Clearly, this behaviour will have a direct influence on the structure and therefore the physical properties of the formed web. It is apparent from *Figure 6* that 38% of fibres landed on-end before falling down (Hit-Fall), so that their longitudinal axis was parallel to the belt surface. From this experimental study we can also estimate the total proportion of non-straight fibres (i.e. curved fibres) landing on the conveyor belt, which is effectively the sum of classes D and F, i.e. 23%. Thus, it may be concluded that the majority of fibres deposited on the belt possessed a straight (rod-like) fibre configuration.

In *Figure 7*, classification of the fibre landing configurations in six different positions along the length of chamber are shown in order to demonstrate how the sampling position affects the reproducibility of the results. It was observed that while variation is apparent, the general trend remains the same. The majority of fibres fall into classes B or C irrespective of the position along the length of chamber.

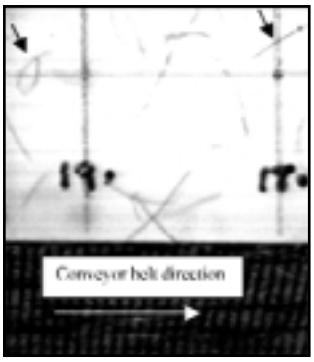

First image

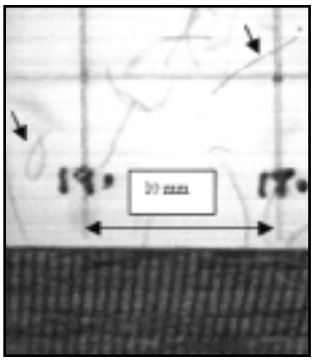

Fibre images after 3.3 millisecond

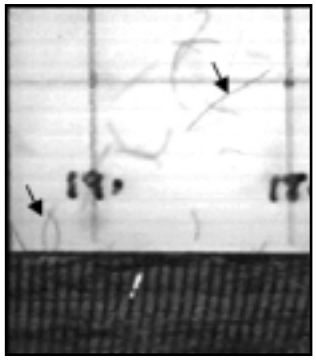

Fibre images after 6.2 millisecond

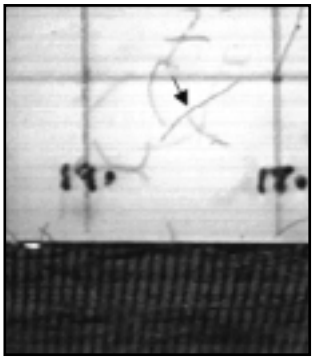

Fibre images after 7.8 millisecond

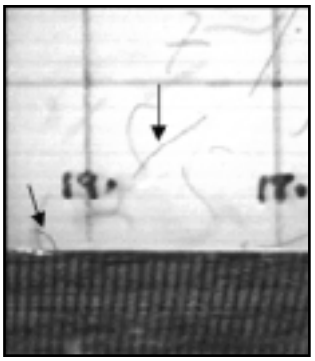

Fibre images after 10.4 millisecond

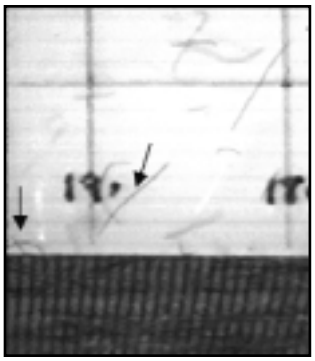

Fibre images after 14.2 millisecond

Figure 4
FIBRES IN THE LANDING AREA

Determination of the Fibre Landing Angle

The landing angle of fibres on the conveyor belt was also obtained using the geometric method indicated in *Figure 8*.

The angle (a) between the fibre line (i.e. the line AB in *Figure 8*, which joins the two ends of the fibre) and the conveyor belt is described as the fibre landing angle.

Figure 9 shows frequency distributions for the fibre landing angle taken at positions Y = 280-350 mm along the length of the chamber using the standard machine conditions and raw materials described in Part I. It may be observed that the majority of fibres land with an orientation of about 100-140^0 relative to the conveyor belt. This is connected with the well-known non-planar structural architecture of many air-laid fabrics where fibres are orientated in three dimensions, producing bulky, low-density structures.

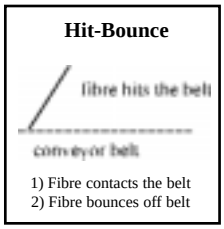

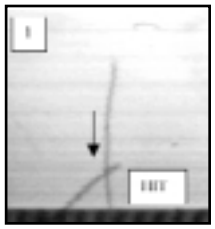

First image

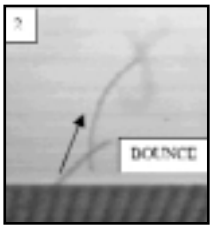

after 2.9 millisecond

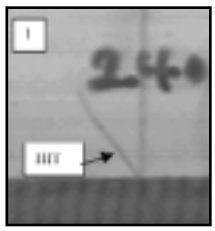

First image

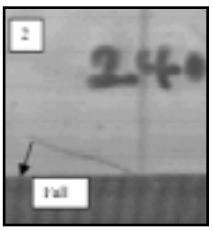

after 3.8 millisecond

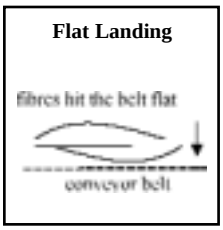

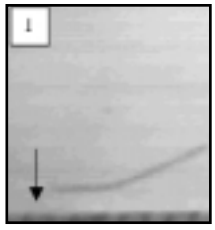

First image

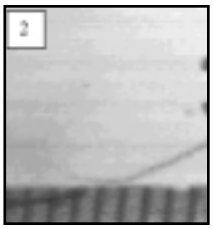

after 2.2 millisecond

Figure 5a
FIBRE LANDING CONFIGURATIONS
ON THE CONVEYOR BELT

Figure 5b
FIBRE LANDING CONFIGURATIONS
ON THE CONVEYOR BELT

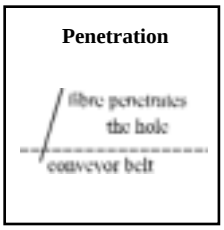

First image

after 3.6 millisecond

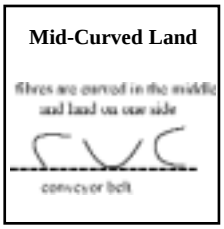

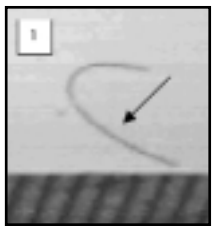

First image

after 3.6 millisecond

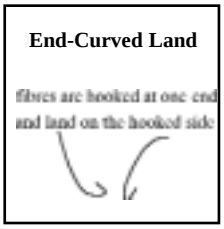

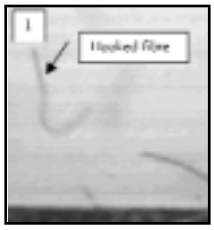

First image

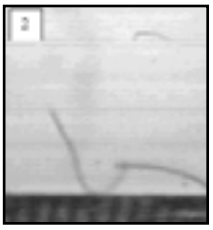

after 2.2 millisecond

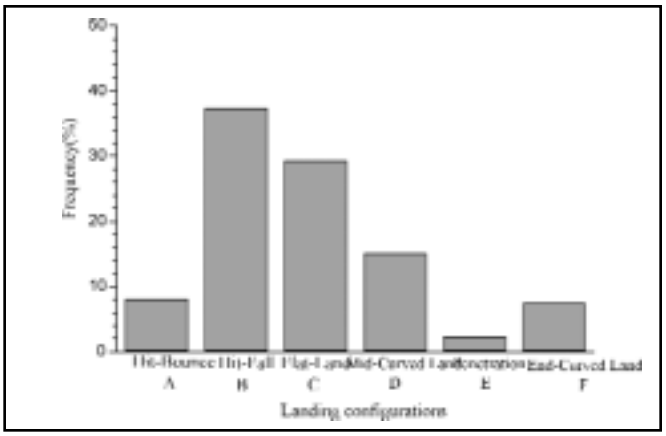

Figure 6
OVERALL FREQUENCY DISTRIBUTION OF FIBRE LANDING CONFIGURATIONS ON THE CONVEYOR BELT

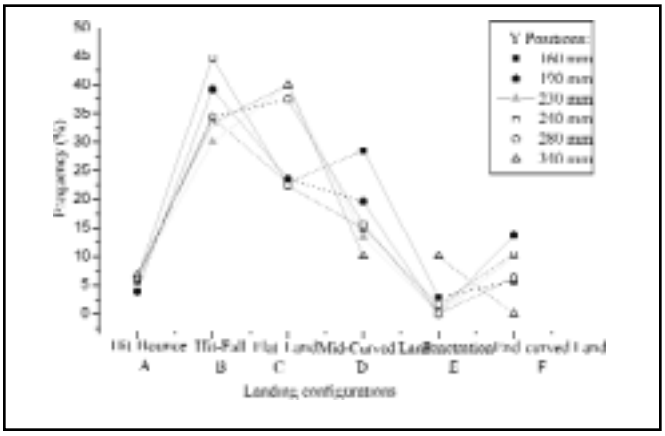

Figure 7
FIBRE LANDING CONFIGURATIONS IN DIFFERENT POSITIONS ALONG THE LENGTH TRANSPORT CHAMBER (Y DIRECTION)

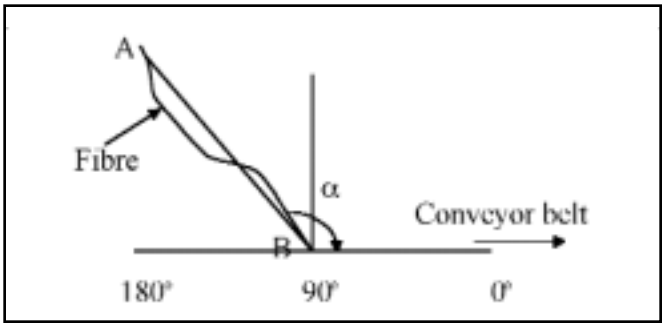

Figure 8
METHOD OF MEASURING THE FIBRE LANDING ANGLE

Conclusions

Air-laid technology continues to be a major growth area in the nonwoven industry. Web uniformity and fabric properties will partly depend on an improved understanding of the web formation process and this article has explored some of the characteristics of the fibre dynamics in a short fibre air-laying system.

For the settings used, it has been revealed that at the top of the transport chamber fibres rotate intensively in all planes showing three-dimensional motion with variable velocities ranging from 0.5-2.0 m/s. In the landing area, if fibres hit the empty belt, it was found that 38% of all fibres land on-end before falling down (Hit-fall configuration) onto the conveyor belt and about 30% of fibres first land flat before bouncing and coming to rest. It was also concluded that a minority of fibres (23%) possess a curved or hooked configuration in the landing zone and that this curvature was imposed by passage of the fibres through the top grid. On an empty conveyor belt the fibre landing results showed that the majority of fibres land with an orientation of about 100-140 relative to the conveyor belt. When incoming fibres deposit on an existing fibre layer their approach configurations tend to be retained.

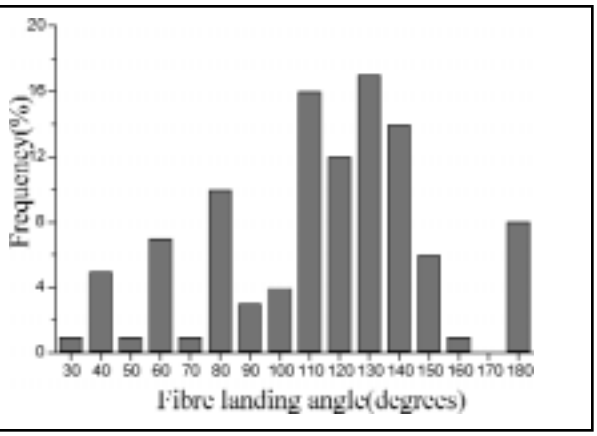

Figure 9
FIBRE LANDING ANGLES ALONG THE LENGTH OF CHAMBER

Acknowledgements

The authors gratefully acknowledge the support provided by EPSRC and to our collaborating industrial partners (ConvaTec Ltd Wound Healing Research Institute and Ulster Carpet Mills). Thanks are also due to our colleague Mr. M. Phillips of the Nonwovens Research Group.

References

Allen K.J. "Friction spinning: An investigation of yarn formation," PhD thesis, Loughborough University 1991.

Kroyer, K. "Dry-laying a web of particulate or fibrous material," USP 4,144,619 (1979).

Lawrence C.A. and Chen K.Z. "A study of the fibre transfer-channel design in rotor-spinning," *J. Text. Inst.* Vol.79, No.3, PP367 (1988).

Lawrence C.A. and Jiang R.K. "A study of mechanics of fibre-straightening during deposition in the disc-spinning process Part II," *J. Text. Inst.* Vol.87, No.1, PP37 (1996).

Pourmohammadi, A, "Fibre dynamics in air-laid nonwoven process," Ph.D. thesis, Leeds University, 1998.

— INJ

Strength Loss In Thermally Bonded Polypropylene Fibers

By Aparna Chidambaram, Hawthorne Davis and Subhash K. Batra,
College of Textiles, North Carolina State University, Raleigh NC

Abstract

Single fiber experiments to analyze the relationships between fiber structure, fiber properties and bonding conditions were performed with three structurally different polypropylene (PP) fibers. Bonds were formed between pairs of fibers at different temperatures and bond strengths were measured. Fiber strengths were measured before and after bonding to estimate changes caused by the bonding process. Bonded fiber strength was also compared with the strength of single fibers which experienced the same thermal conditions to assess the effect of mechanical damage from pressing fibers together with steel rolls while creating bonds. In all fiber types, significant bonding occurred simultaneously with degradation of fiber strength. The observed reduction in fiber strength was caused mainly by thermal, rather than mechanical, damage during bonding. Fibers with low birefringence skins formed strong interfiber bonds at lower temperatures with smaller losses in fiber strength.

Introduction

In thermal point bonding (TPB), direct contact between small, heated, raised metal islands on an engraved calender roll and a nonwoven web produces localized bonding together of the fibers. This process converts a weak web of fibers into a tenacious fabric. Typically, the bond points amount to 20% of the fabric area. Fabric strength is determined by both the strength of the bonds and the residual strength of bridging fibers which run between bonds. Other effects, such as inhomogeneous straining and cooperative loading, are doubtless also important.

A well-documented observation in TPB studies is that the fabric strength, generally measured parallel to the machine direction (MD), is highest at an optimum bonder temperature which is lower than the maximum that will run without melting the fabric [3, 6, 7, 11].

Dharmadhikary et al. [3] explained this maximum in fabric strength as the result of increasing bonder temperatures increasing adhesion on one hand while reducing fiber strength on the other. This explanation differed from previous work [6,7,13], which attributed fabric strength degradation beyond the optimum to pseudo-metallurgical effects such as "defects" and "embrittlements."

Strength loss of 19 to 35% was directly measured in bridging fibers after bonding in [3]. The nature of this fiber strength loss, which corresponds with a substantial amount of wasted polymer in the large, lightweight nonwovens market was, however, unclear. Dharmadhikary et al. [3] measured bridging fiber strengths at different bonding temperatures, but their experiments assessed neither the effect of temperature on interfiber bonding nor the possibility that mechanical rather than thermal damage to the fibers was the main effect.

The present paper describes work to measure and understand the strength of interfiber bonding and fiber strength degradation under conditions which reasonably simulate TPB. This article concentrates on polypropylene (PP) fibers.

Experimental Details

Materials

Three different types of PP fibers were studied.

T196 is a high-performance, single component fiber manufactured specifically for TPB by Fiber Visions Inc. These fibers were received "as produced" *viz*. with the commercial spin finish. To evaluate the effect of the finish on bonding, we compared as-received fibers with fibers from which finish had been extracted using 2-propanol. It was known from previous work [3] that T-196, although a single component polypropylene fiber, has been subjected to a treatment in manufacturing which gives it a bonding-enhancing surface region.

Two varieties of experimental, finish-free, bicomponent fibers were obtained from Kimberly-Clark

Polypropylene Sheath/Polypropylene Core (PP/PP) fibers, which had the same polymer in sheath and core, simulated a normal, homopolymer fiber with no adhesion-enhancing surface layer. A 3% ethylene/ 97% propylene random copolymer sheath/homopolymer PP Core fiber (RC/PP) product of the same linear density was used as a second example of inho-

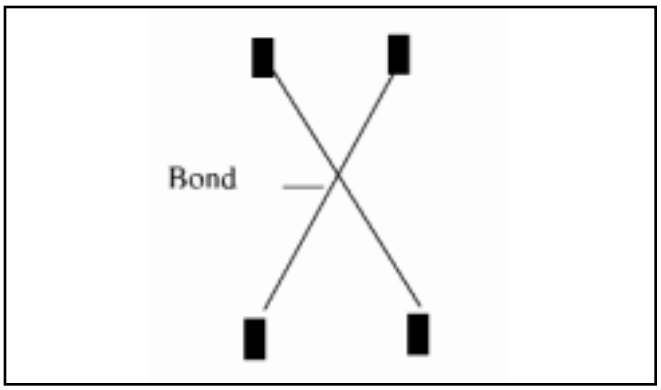

Figure 1
SCHEMATIC OF FIBER ARRANGEMENT FOR PRODUCING BONDED PAIR SPECIMENS

mogeneous fiber, which was expected to differ from the other two items due to its different surface layer.

Bonding Experiments

A method for bonding pairs of fibers and measuring interfiber bond strength, as well as changes in fiber strength after bonding, was utilized in this work. The procedure adopted approximates normal TPB process conditions more closely than previously reported work. Whitwell et al. [14] used an infrared laser to bond two crossed over monofilaments, while Mukhopadhyay and Foster [10] bonded two interlooped fibers with hot air. Neither of these processes approximates the bonding pressure and short contact times (~8-20 milliseconds) of real processes. Kennedy [9] bonded crossed-over pairs of fibers by attaching them to Kraft paper and exposing them to heated calendering. Presumably Kennedy also tested the resulting fibers, but his work was never published. This method was judged the best available approximation to actual TPB, which left fibers available for study, and it was implemented for our work. Since experimental details were not available, exact methodology had to be developed again. The methods ultimately implemented are described below.

Specimen Preparation

Two types of specimens were prepared: (1) bonded fiber pairs and (2) control fibers. In "bonded pairs" two fibers crossed over at a 45^0 angle and were attached, with slight amount of slack, to 40 lb. Kraft paper, with glue as in *Figure 1*. The Kraft paper with attached fiber pairs was run between smooth, oil-heated calender rolls at controlled temperatures, speeds and pressures. Smooth rolls guaranteed contact at the crossover point where an interfiber bond formed. "Control fibers" were single fibers attached to Kraft paper as shown in *Figure 2* and subjected to the same calendering.

To assess whether the Kraft paper backing affected fiber strength, single fibers were attached across a hole cut in Kraft paper as shown in *Figure 3* and calendered at various temperatures. These specimens, termed "direct" fibers, ensured that fibers were not pressed against the paper. For control vs. direct fiber comparison, both kinds of specimens were attached to the same piece of Kraft paper.

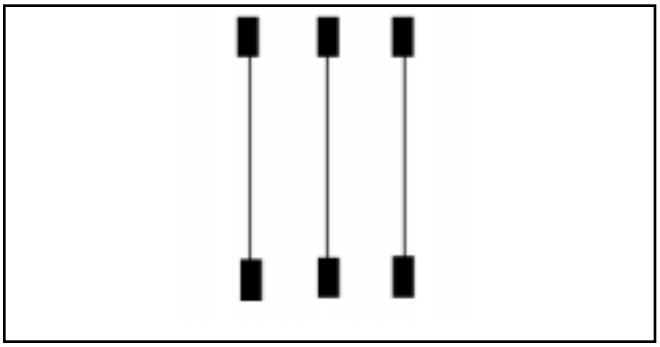

Figure 2
SCHEMATIC OF ARRANGEMENT FOR PRODUCING CONTROL FIBER SPECIMENS

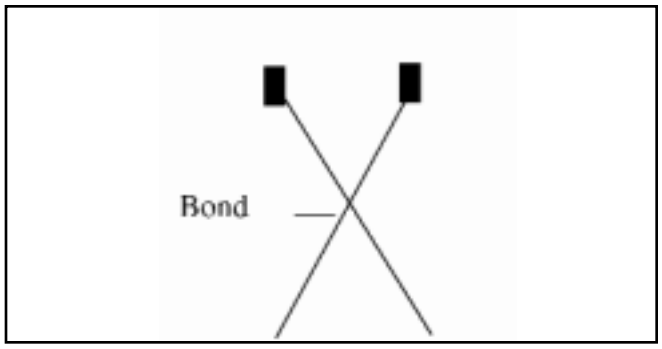

Figure 3
SCHEMATIC OF ARRANGEMENT FOR PRODUCING DIRECT FIBER SPECIMENS

Bonding Conditions

Of the three available process variables, temperature, pressure and roll speed, only temperature was varied in this work. Prior studies [1, 2] had showed pressure was not a particularly important variable in bonding, and roll speed was set to give a commercially realistic contact time of 9 ms. A critical temperature range was identified for each item tested based on scouting experiments, and this range was studied in detail. *Table 1* lists bonding temperatures used for each fiber type. Eighty to 100 bonded pairs of each fiber type were made for bonding at each condition. Of these, 30-50 pairs actually

Table 1
FIBERS AND BONDING CONDITIONS
(Pressure: 19 kN/m (108 lbs/linear inch); Speed: 0.3 m/sec (56 ft/min))

Fiber Type	T196 (With and Without Finish	RC/PP	PP/PP
Linear Density (denier)	2.68	4	4
Roll Temperatures, ^{0}C	123,127,131	120,128,132	137,143

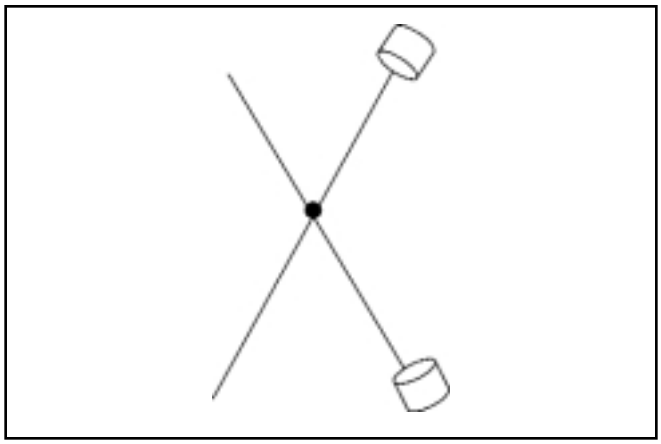

Figure 4
SCHEMATIC OF ARRANGEMENT FOR MEASURING BOND STRENGTH. THE 'CYLINDERS' REPRESENT CLAMPS OF THE TENSILE TESTING MACHINE

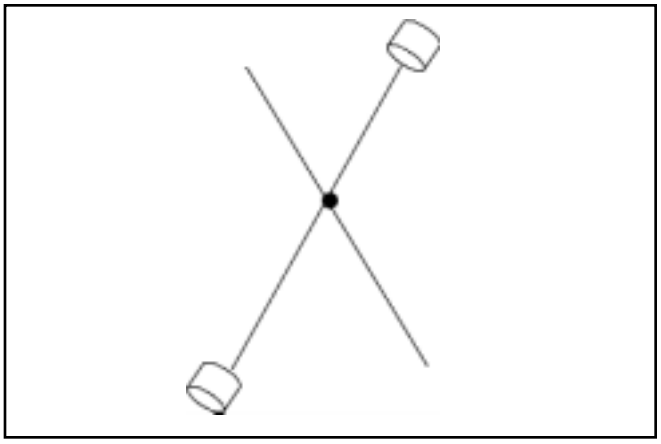

Figure 5
SCHEMATIC OF ARRANGEMENT FOR MEASURING THE TENSILE STRENGTH OF BONDED FIBERS. 'CYLINDERS' REPRESENT CLAMPS OF TENSILE TESTING MACHINE

bonded together and were used in experiments. The rest were ignored.

Fibers used in this work did not seem to stick to the Kraft paper. In other work, not reported here, fibers with polyethylene sheaths did stick to the paper and could not be used for this type of investigation.

Testing of Bonded Pairs and Fibers

A constant rate of extension Instron was used to test fiber and bond strengths. A 5 mm gage length and cross head speed of 5 mm/min were used for all tensile tests. After calendering, the pairs which actually bonded were cut at their ends, to separate them from Kraft paper, and tested for residual fiber strength and bond strength. Bond strength was evaluated by stressing the bond as shown in *Figure 4*, where one end of each fiber was clamped and stretched to separate the bonded fibers at the interface. The maximum force developed was defined as bond strength. Fiber strength after bonding was measured by straining one of the fibers in a bonded pair, including the bond region until it fractured *(Figure 5)*. The maximum force before fiber failure per unit linear density of the fiber was recorded as fiber tenacity. As-received, control and direct fiber tenacities were measured in the same way, except there was no bonded region in the specimen.

Microscopy of Fibers and Bonds

Interference Microscopy of As-Supplied and Direct Fibers

An *Aus Jena* interference microscope was used to evaluate the radial variation of the principal refractive indices in the fibers. The method is based on Wu et al. [15]. A straightforward, refraction corrected sheath/core ray tracing analysis, which is anticipated but not explicitly covered in [15], was used to analyze the sheath/core fibers. Knowing the principal refractive indices allows calculation of birefringence

$$(n\parallel - n\perp)$$

and isotropic refractive index

$$\frac{n\parallel + 2n\perp}{3}$$

at any radial position, within the fiber, or alternatively in the sheath and core, depending on the analysis used.

Scanning Electron Microscopy (SEM) and Polarized Light Microscopy

Bonded pairs were examined with a Hitachi S-3200N SEM after being coated with a thin layer of gold. Bonds were viewed from top and bottom. Surfaces of fibers, which had been separated from their partners in the bonded pair in tensile tests, were also scanned in detail to find the area where the bond had existed. A polarizing light microscope was used to examine fibers calendered with Kraft paper backing and direct fibers for damage.

Results

All quantitative comparisons reported have been subjected to appropriate statistical tests and satisfied a confidence level of at least 90%.

SEM Study of Bonded Pairs

SEM photographs of bonded pairs are shown in *Figures 6 and 7*. *Figure 6* shows the bond from above. *Figure 7*, which views the same bonded pair from below, clearly indicates some flow at the edges. *Figures 8 and 9* show fibers separated from their bonded partners. These suggest that bonding occurred mainly at the edges of the contact region, where some roughness can be seen.

Effect of Temperature on Bond Strength

The average bond strength for each fiber type always increased with bonding temperature over the range tested

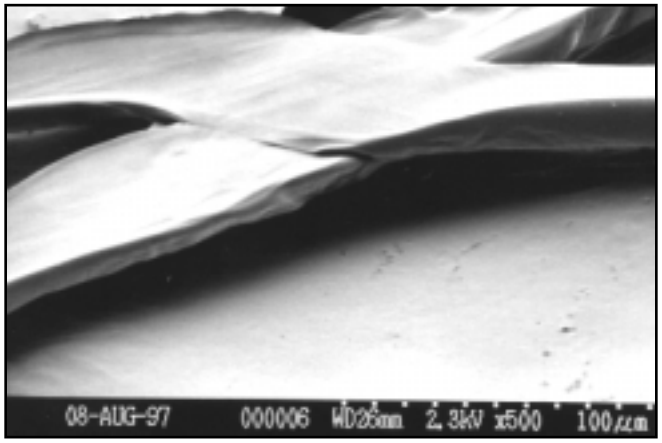

Figure 6
SCANNING ELECTRON MICROGRAPH SHOWING TOP (I.E. SURFACE CONTACTING ROLL) OF CROSSED FIBER BOND

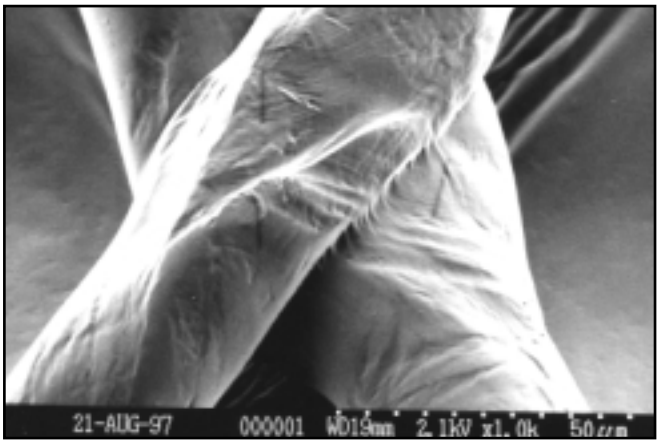

Figure 7
SCANNING ELECTRON MICROGRAPH SHOWING SIDE OF CROSSED FIBER BOND WHICH WAS IN CONTACT WITH KRAFT PAPER

(Tables 2a and 2b). Strong bonds formed at the highest temperatures used. Data in every case had high coefficients of variation (~35 to 70%). However, statistical tests always confirmed increases in bond strength with temperature.

Bond strengths of T196 fibers were adjusted to compensate for their diameters (~10 μ) for comparison with RC/PP and PP/PP diameters (~25 μ diameter), as will be described below. Smaller diameters of T196 fibers would normally result in smaller contact areas at the bond point (or crossover point). Since bonding was observed mainly at the edges of a rhomb-shaped contact area (*Figures 6-9 and Figure 10* schematically), the actual bonded region was assumed proportional to the perimeter of the rhombus, which is approximately proportional to the square root of linear density (in denier). Therefore, T196 bond strengths were adjusted by multiplying measured data by the square root of the ratio of linear densities of the fibers ($\sqrt{4/2.68} = 1.22$) for reasonable comparison with the other items. Even with this correction, T196 appears to form weaker bonds than the other fibers, but further testing would be required to confirm this as an established experimental result.

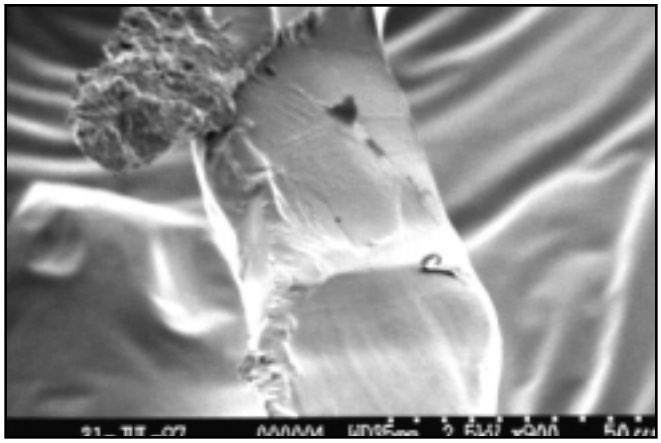

Figure 8
SCANNING ELECTRON MICROGRAPH SHOWING SEPARATED BOND

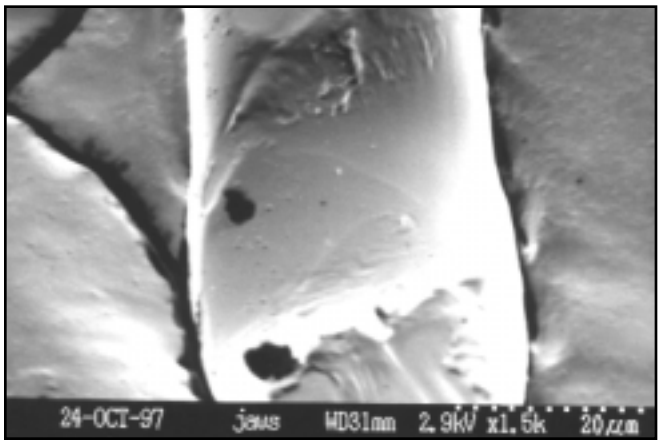

Figure 9
SCANNING ELECTRON MICROGRAPH SHOWING SEPARATED BOND

Table 2a
BOND STRENGTH (GF) (STANDARD DEVIATION IN BRACKETS): T196

Type	123°C	127°C	131°C
With Finish	0.42 (0.3)	0.72 (0.33)	1.18 (0.45)
No Finish	0.54 (0.36)	1.09 (0.44)	1.54 (0.58)

Table 2b
BOND STRENGTH (GF) (STANDARD DEVIATION IN BRACKETS): PP/PP AND RC/PP

Type	120°C	128°C	132°C	137°C	143°C
PP/PP	—	—	—	0.58(0.3)	2.09(1.3)
RC/PP	0.42(0.33)	1.19(0.47)	2.25(1.37)	—	—

Effect of Finish on Bond Strength of T196 Fibers

As can be seen in *Table 3*, T196 fibers with commercial

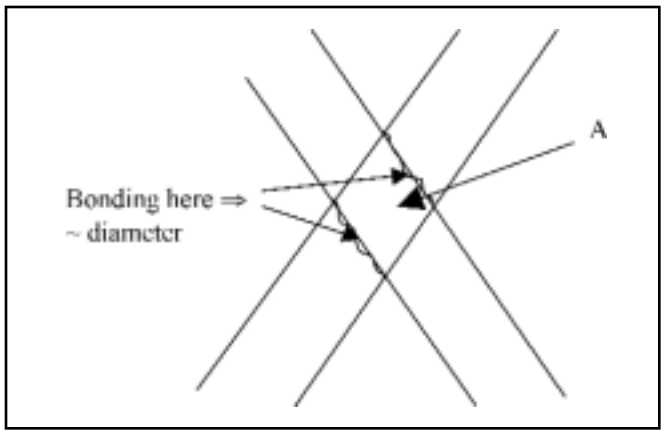

Figure 10
SCHEMATIC OF BONDED REGION BETWEEN TWO CROSSED OVER FIBERS

Table 3
BONDED FIBER TENACITY (GF/DEN): T196 (STD. DEV. IN BRACKETS)

Type	As-Supplied	123°C	127°C	131°C
With Finish	1.6 (0.14)	1.55 (0.14)	1.46 (0.18)	1.42 (0.14)
No Finish	1.54 (0.18)	1.48 (0.11)	1.46 (0.12)	1.41 (0.19)

Table 4
BONDED FIBER TENACITY (GF/DEN): PP/PP AND RC/PP (STD. DEV. IN BRACKETS)

Fiber	Supplied	120°C	128°C	132°C	137°C	143°C
RC/PP	2.45(0.44)	2.68(0.4)	2.68(0.42)	2.4(0.57)	—	—
PP/PP	2.61(0.29)	—	—	—	2.42(0.17)	2.03(032)

Table 5
COMPARISON OF BONDED AND CONTROL FIBER TENACITIES (GF/DEN): T196 (STD. DEV. IN BRACKETS)

	123°C		127°C		131°C	
Type	Bonded	Control	Bonded	Control	Bonded	Control
With Finish	1.55 (0.14)	1.53 (0.17)	1.46 (0.18)	1.47 (0.16)	1.42 (0.14)	1.38 (0.2)
No Finish	1.48 (0.11)	1.6 (0.13)	1.46 (0.12)	1.53 (0.1)	1.41 (0.19)	1.45 (0.22)

spin finish consistently formed weaker bonds than those from which finish had been extracted.

Effect of Temperature on Bonded Fiber Strength

Table 4 compares the effect of increasing temperature on bonded fiber strength for the items studied. T196 and PP/PP fibers became weaker after bonding. This strength loss increased as temperature of bonding increased. PP/PP fibers suffered >20% loss in tenacity at the highest bonding temperature, which was needed to form reasonably strong bonds. Comparatively, T196 fibers lost only 10% of their tenacity at the highest temperature used to form strong bonds. Unlike T196 and PP/PP fibers, RC/PP fibers increased in tenacity at 120°C and 128°C, and at 132°C had the same strength as the as-supplied fibers. Although RC/PP fibers formed strong bonds at 132°C without losing strength relative to the as-received state, they did lose strength over the temperature range required to produce bonds. Fiber lengths were constrained by Kraft paper during bonding to approximate TPB manufacturing. This was expected to maintain fiber linear density and to minimize deorientation. No measurements were made to verify the constant linear density. A small effect of constrained heating on birefringence of RCPP fibers is reported in *Table 9*.

Cause of Fiber Strength Degradation

Damage from Bonding

Bonded fiber tenacities were compared with those of control fibers at the same bonding conditions to assess the effect of mechanical damage during bonding on fiber tenacity *(Tables 5 and 6)*. No statistically significant difference was detected between bonded and control fiber tenacities for a given fiber type and bonding condition. This indicates that heat-treated fiber tenacity does not depend on whether the fiber is heated by itself, flat on a paper or crossed over and pressed against another fiber sufficiently to cause extensive deformation.

Embossing from Kraft Paper: Cause of Reduction in Fiber Strength

The undersides of bonded fibers upon observation in the SEM showed a severely damaged or "embossed" surface. To determine if the Kraft paper backing was responsible for this embossing, direct fibers were examined under crossed polars in a light microscope. As described earlier, direct fibers were calendered at conditions similar to control fibers but while attached across a hole cut in the Kraft paper. This arrangement brought the fibers into direct contact with the calender rolls, unlike the bonded and control fibers, which had Kraft paper between them and the rolls. *Figures 11 and 12* compare the apparent damage to Kraft and direct fibers using polarized light microscopy. No evidence for embossing is present in the direct fibers. This indicates that the Kraft paper "damaged" the undersides of bonded and control fibers.

To assess if this embossing contributed to fiber strength degradation, sets of direct and control fibers were calendered over a range of temperatures. Strengths of both, direct and control, fiber specimens were compared *(Table 7)*. No significant difference in strength was found between direct and control fibers at a given calendering temperature. Evidently, embossing from Kraft paper, a form of mechanical damage

Table 6a
COMPARISON OF BONDED AND CONTROL FIBER TENACITIES (GF/DEN): RC/PP (STD. DEV. IN BRACKETS)

120°C		128°C		132°C	
Bonded	**Control**	**Bonded**	**Control**	**Bonded**	**Control**
2.68 (0.4)	2.6 (0.41)	2.68 (0.42)	2.8 (0.5)	2.4 (0.57)	2.38 (0.3)

Table 6b
COMPARISON OF BONDED AND CONTROL FIBER TENACITIES (GF/DEN): PP/PP (STD. DEV. IN BRACKETS)

137°C		143°C	
Bonded	**Control**	**Bonded**	**Control**
2.42 (0.17)	2.41 (0.24)	2.03 (0.32)	2.1 (0.27)

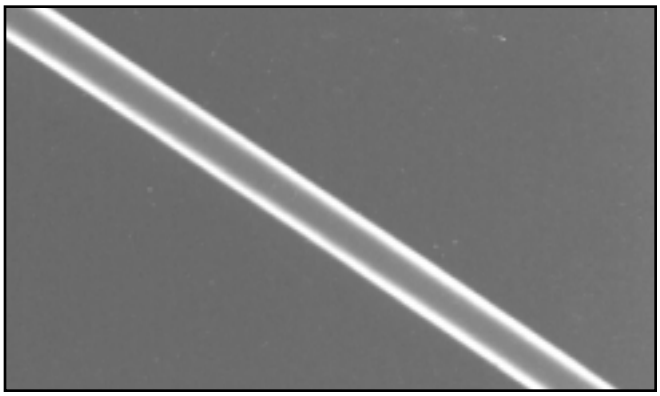

Figure 11
VIEW OF DIRECT FIBER BETWEEN CLOSED POLAROIDS

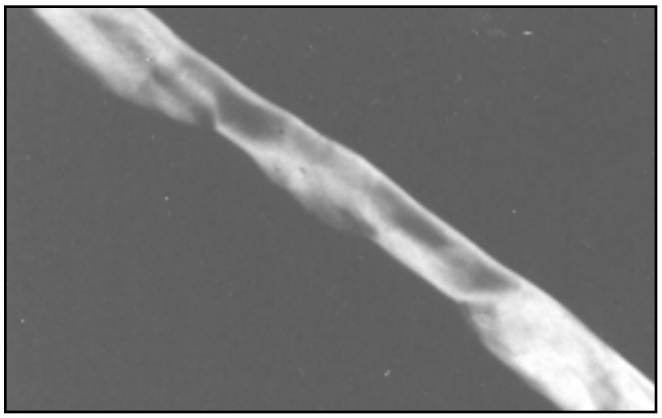

Figure 12
VIEW OF CONTROL FIBER BETWEEN CROSSED POLAROIDS

which at least looks severe, is not a detectable contributor to fiber strength loss under conditions appropriate to TPB.

Interference Microscopy of Fibers

A skin of low birefringence was readily detected on T196 and RC/PP fibers *(Table 8)*. This skin had extremely low birefringence compared to that at the center The surface or skin of PP/PP fibers, on the other hand, had slightly higher birefringence than the core.

Increasing strength of RC/PP fibers with temperature

An attempt was made to investigate the increase in strength of RC/PP fibers upon calendering at 120 and 128°C. Direct RC/PP fiber samples were calendered over a range of temperatures. Their tenacities and refractive indices were measured. RC/PP fibers increased significantly in strength at 120°C but deteriorated severely at 140°C *(Table 9)*. At 120°C, a detectable rise in core isotropic refractive index and birefringence was also noted. Isotropic refractive index can be directly correlated with density of fiber [8] and is an orientation independent measure of crystallinity. Birefringence is not, however, a crystallinity-independent measure of orientation. Therefore, the increase in strength of RC/PP fibers at 120°C might be associated with this increase in core density. The strength of RC/PP fibers does, however, reduce significantly upon heating at 140°C.

Statistical Distribution of Fiber Strength Data

As-received and bonded fibers' strengths, were fit reasonably by the two parameter Weibull distribution:

$$\ln (- \ln (1- P_f (\sigma))) = \ln (N) + M \ln (\sigma/\sigma_0),$$

where $P_f (\sigma)$ is the probability of failure at stress σ, N is the number of flaws, M is the fitting parameter or Weibull Modulus and σ_0 is related to the average strength. A plot of $\ln (- \ln (1- P_f (\sigma)))$ against ln (fiber strength) has a slope of 1/M. Such plots were made for each fiber and bonding condition to find 1/M values *(Table 10)*. A higher value of 1/M indicates a broader distribution of strengths, which is often interpreted as the presence of more severe flaws.

For all fiber types, Weibull modulus values after bonding were higher than for as-supplied fibers, indicating that the apparent density of "flaws" increased after bonding. This

Table 7
COMPARISON OF RC/PP DIRECT AND CONTROL FIBER PEAK LOADS (GF)

Temperature, °C	Direct Fiber (gf) (Std. Dev.)	Control Fiber (gf) (Std. Dev.)
As-Supplied	10.76 (1.3)	10.76 (1.3)
25 (Cold Rolls)	11.03 (1.77)	11.3 (0.4)
100	11.33 (1.79)	11.73 (1.8)
110	10.46 (2.26)	9.79 (1.22)
120	11.54 (1.88)	10.38 (1.64)
125	10.1 (2)	11.09 (1.96)
130	11.36 (2.12)	10.62 (1.15)
135	7.88 (1.07)	8.68 (1.28)
140	8.08 (1.1)	—

Table 8
BIREFRINGENCE AT SURFACE AND CORE OF AS-RECEIVED FIBERS

Fiber Type	Model	Surface	Core
T196: No Finish	Sheath-Core	0.008	0.022
RC/PP	Sheath-Core	0.009	0.025
PP/PP	Continuous	0.029	0.025

Table 9
TENACITY AND OPTICAL PROPERTIES OF RC/PP DIRECT FIBERS AS IT DEPENDS ON TREATMENT TEMPERATURE (STD. DEV. IN BRACKETS)

Temperature	Tenacity (gf/den) Std. Dev. in Parentheses	Core Birefringence	Core Isotropic Refractive Index
As-Received	2.45 (0.4)	.0248	1.5019
100	2.79 (0.6)	.0241	1.5032
110	2.41 (0.5)	.0259	1.5033
120	2.88 (0.54)	.0260	1.5043
140	1.49 (0.39)	.0271	1.5073

Table 10
WEIBULL SLOPES FOR AS-SUPPLIED AND BONDED FIBERS

Fiber Type	Before Bonding	After Bonding		
T196 No Finish	0.11	0.06@123°C	0.08@127°C	0.13@131°C
T196 With Finish	0.09	0.09@123°C	0.13@127°C	0.08@131°C
RC/PP	0.04	0.08@120°C	0.1@128°C	0.11@132°C
PP/PP	0.1	0.12@137°C	0.15@143°C	

Table 11
APPARENT ACTIVATION ENERGIES FOR BOND FORMATION AND STRENGTH LOSS (KCAL/MOLE)

Type	Bonding	Fiber Strength Loss
T196 No Finish	42	31
T196 With Finish	41	51
PP/PP	72.4	63

observation confirms similar results of [3] using a completely different approach.

Activation Energy

An attempt was made to estimate apparent activation energies for bonding and fiber strength degradation. This analysis was based on molecular rate process theories of fracture, which describe materials to be made up of elements whose failure is related to the macroscopic fracture of materials. Failure is assumed to be a rate process described by the Arrhenius relationship (given below) determined by thermally activated fracture of primary and/or secondary bonds within the material.

$$k = A \exp (- \Delta E/RT)$$

where, k is a rate constant, A is the frequency factor, ΔE is the empirical activation energy, R is the gas constant and T is the absolute temperature. In this analysis, bond formation as well as fiber strength loss were assumed to be rate processes. Bonding activation energies were calculated using the increase in bond strengths as temperature increased. Activation energies for fiber degradation were calculated from the increase in fiber strength loss (relative to as-supplied fiber strength) with increasing bonding temperature. The values are not extremely accurate since only three data points were available for each estimate. *Table 11* shows the values obtained. The energies for bond formation and strength loss are similar for a given fiber type. Energies for RC/PP fibers were not calculated since RC/PP fibers increased in strength at intermediate temperatures, and it was not possible to apply the analysis.

Discussion

The results reported generally agree with measurements and qualitative observations of Dharmadhikary et al. [3]. The method reported here is the only one we are aware of for evaluating the effect of TPB on individual fibers and inter-fiber bonding under conditions which reasonably simulate commercial practice. Contact times were on the same order (~9 milliseconds) as those reported for industrial processes (8-20 milliseconds). The temperatures at which bonds formed between pairs of fibers were lower than bonding temperatures typically used for fabrics. This might be attributed to the fact that only two fibers are being bonded in the current study whereas in a fabric, large numbers of fibers cluster together at a bond point. The contact pressure used in this study was not accurately known, but actual contact pressures are also not accurately known in industrial processes.

Based on observations with all PP fiber types used here, a common thread is seen *viz.* the concurrent processes of increasing bond strength and degradation in fiber strength within the same temperature range. This is clearly seen in *Figure 13*, which compares the temperature dependence of bond and fiber strengths for the items studied. The data points, all taken from tables in this paper, are not shown on *Figure 13* to reduce clutter. Untreated fiber strengths were

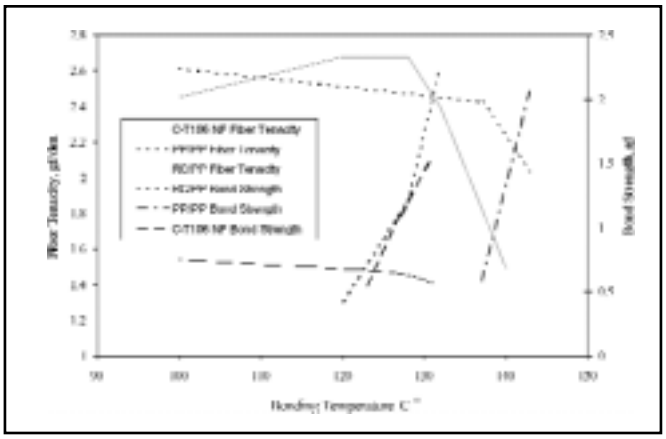

Figure 13
COMPARISON OF BOND STRENGTH WITH RESIDUAL FIBER STRENGTH FOR ALL ITEMS IN THE EXPERIMENTS

plotted at 100°C to compress the temperature scale for clarity. While these do not represent actual data points, it is known from various results *(e.g. see Table 9)* that constrained, millisecond heat treatment at 100°C has no detectable effect on fiber or bond strength. These two effects *viz.* increasing bond strength and decreasing fiber strength also have indistinguishable apparent activation energies, within the accuracy of the experiments, suggesting both probably depend on the same unit process.

While all three fiber types formed strong bonds, the conventional PP/PP variety suffered large losses in fiber strength at the high (i.e. 143°C) temperatures required. T196 fibers lost less strength, mainly because they bonded at lower temperatures. RC/PP fibers had no net loss in strength at the highest bonding temperature used, although strength was in fact dropping over the temperature range where strong bonds formed. This intermediate temperature strength increase of RC/PP fibers corresponded with detectable changes in core refractive indices, a significant quantitative indication of structure changes. T196 and RC/PP fibers have a low birefringence sheath, which enabled bonding at significantly lower temperatures than PP/PP. This is the likely origin of their smaller losses in strength during bonding.

Goraffa et al. [7] speculated that a "stress concentration" may exist at the bond perimeter due to "crush damage," which reduces fiber strength. Another form of mechanical damage exclusive to the current study was the embossing from Kraft paper used as backing. We attempted to establish mechanical damage as a detectable cause of strength loss in bonding, but no evidence in favor of this hypothesis was found. The possible causes of strength loss in these experiments were thermal and mechanical damage, and it must therefore be concluded that thermal damage is the main culprit. It is commonly known that PP undergoes thermo-oxidative degradation upon exposure to oxygen and high temperatures, both of which are present during TPB. We do not mean to imply that thermally induced molecular weight loss is necessarily involved in this case, however.

Proposed explanation

Although quantitative theory is elusive, it is clear that our results are to be expected based on what everyone knows about fiber microstructure. Recourse to vague metallurgical concepts is not needed. Based on work like that of Davis [5], it is clear that the various "models" of fiber structure, apart from the highly unlikely "coil" model of Davidovits [4], reduce to the same functional structure. Functionally a fiber is an anisotropically connected network of polymer molecules, in much the same way that a TPB nonwoven is a network of fibers. The nodes in the fiber's network are crystals (and possibly entanglements), while the connectives are segments of polymer molecules which run between nodes. Tenacity in such a network depends on effective use of the intrinsically high strength of the connectives, which in turn requires 1) the nodes to be strong (i.e. large enough) and the 2) connectives to be sufficiently uniform in length to bear load cooperatively. To bond two such networks (i.e. two fibers) requires diffusion of chain segments from each across the interface between them. This process requires the connectives to be free, at least on one end, or possibly only able to form a long loop, either of which intrinsically disrupts network connectivity. Confining this chain segment freedom to a small region near the interface, e.g. by having it melt or soften at a lower temperature than the fiber core, could yield significant bonding with minimal loss of tenacity, i.e. minimal disruption of the network in the fiber core. In a homogeneous fiber, e.g. like the PP/PP fiber in this work, freeing up connectives near the surface simultaneously frees up connectives in the fiber core, which intrinsically costs connectivity and strength due to well understood polymer chain segment behavior.

Mechanical damage

Mechanical damage to fibers can occur when the fibers are squeezed together or when they are pressed into the Kraft paper in our experiments. We showed that both forms of mechanical damage contributed little to fiber strength loss. Bonded fiber strengths were not different from control fiber strengths. Additionally, direct fibers suffered similar strength losses as embossed (or control) fibers. By eliminating mechanical damage as a significant factor in fiber degradation, this study indicates that strength reduction in fibers results primarily from the heat required to effect bonding.

Magnitude of bond strength

An attempt was made to project results from bonded pair tests to fabric bonds: the shear strength of a bonded pair was estimated to be 800 gf/mm^2 by using an average interfiber bond strength (at the lowest temperature) of 0.5 gf and assuming the bond contact area to be 25μ*25μ. If this is the shear strength of a 1 mm long fabric bond, the load required to tear this bond would be 20 gf. The average fiber breaking load after bonding at the lowest temperature is ~ 10 gf, indicating that the fiber would fail before the fabric bond. This approximate calculation suggests that it should be relatively easy to produce 1 mm long bonds, as in TPB, that are stronger than the fibers. However, this is not observed in practice, e.g.,

in T196 fabrics bonded at 127°C, bonds failed before the fibers [3]. This apparent discrepancy could arise because bonds formed between the two fibers in the present study represent an idealized situation. Surely, in a fabric not all inter-fiber contacts will form bonds. Further, as mentioned earlier, of the 80-100 specimens subjected to bonding in the current study, bonds formed in only 30-50 cases. Those pairs that did not bond were excluded from the average bond strength data reported here, and such non-bonding present in a TPB fabric bond point would reduce effective bond strength.

Finally, the RC/PP fibers demonstrated the best thermal bonding behavior of the PP varieties evaluated. Their ability to form strong bonds with no net strength loss provides part of the formula to producing a strong TPB fabric. We think this behavior results from perfection of the fiber microstructure, e.g. increase in the size/strength of the nodes (crystals), at intermediate bonding temperatures. It should be pointed out that had the RC/PP fibers required the same bonding temperature as PP/PP fibers, they would have been weaker than bonded PP/PP fibers.

Clapyron effect

Some role of the Clapyron effect, i.e. the increase in melting point due to increasing pressure, has been suspected as a factor in TPB [2]. The electron microscopy shown in *Figures 6-9* seems to indicate that bonding occurs mainly where the pressure is low, i.e. at the edges of the bonds. This phenomenon may explain the known relative insensitivity to bond pressure of TPB processes.

Effect of Finish on Bonding

The presence of finish on fiber surfaces would interfere with the ability of molecule segments to cross the interface. For this reason it should be expected that finish would interfere with bonding, as was observed.

Conclusions

1. The fiber bonding and testing experiment, designed in this study, is effective for directly measuring the effect of various parameters on bond and fiber properties.

2. The bonding process causes degradation of component fiber strengths in the temperature range where significant bonding occurs.

3. The degradation in fiber strength after TPB results mainly from thermal damage occurring during bonding. Mechanical damage due to compaction at bond points or from Kraft paper embossing does not contribute significantly to fiber strength loss.

4. Combined with previous work [3], these observations support the hypothesis that fibers with low birefringence surface layers are preferable to those without such surface layers for TPB because of their ability to form strong bonds without undergoing a significant reduction in fiber strength.

5. Finish, as supplied on T196 fibers, interferes with bond formation producing weak bonds.

Acknowledgements

The authors are grateful for the financial support for this work from the Nonwovens Cooperative Research Center at North Carolina State University, the National Science Foundation and the State of North Carolina.

References

1. Andreassen, E., Myhre, O.J., Hinrichsen, E.L., Braathen, M.D. and Grostad, K., "Relationships between Properties of Fibers and Thermally Bonded Nonwoven Fabrics made of Polypropylene," *Journal of Applied Polymer Science*, 58, p. 1633-1645, 1995.

2. "Thermal Point Bonding of Nonwoven Fabrics," with R. Dharmakhikary and T.F. Gilmore and S.K. Batra, *Textile Progress 26*, No. 2, (1995)

3. R. Darmadhikhary, H. Davis and S.K. Batra, "Influence of Fiber Structure On Properties Of Thermally Point Bonded Polypropylene Nonwovens," *Textile Research Journal*, 69,725, (1999)

4. Davidovits, J., "Morphology of Synthetic Fibers. Model Structures. Probable Mechanism of Formation," *Bull. Sci. Inst. Text. Fr. 1*, 253-270 (1977)

5. Davis, H. "A Theoretical Basis for the Physical Behaviour of Synthetic Fibres," Advances in Fibre Science, Ed. S. Mukhopadhyay, *Text. Inst. 1990*, Chapter VII.

6. Gibson, P.E. and McGill, R.L., "Thermally Bondable Polyester Fiber: The Effect of Calender Temperature," *Tappi Journal*, 70 (12), December, p. 82-86, 1987.[6]

7. Goraffa, A. A-M, Crane, J.P., Iyengar, Y. and Kwok, W.K., "Polyester Staple for Thermally Bonded Nonwovens," Proceedings of the 13th Annual Technical Symposium, Association of the Nonwoven Fabrics Industry (INDA), Boston, MA, p.246-266, 1985.[7]

8. Hermans, P.H., Contribution to the Physics of Cellulose Fibres, Monographs on the Progress of Research in Holland during the War, Houwink, R. and Ketelaar, J.A.A., Editors, Elsevier Publishing Company Inc., p.130-143, 1946.

9. Kennedy, A.D., Personal Communication, 1995.

10. Mukhopadhyay, S.K. and Foster, P.W., "Thermobonding Behavior of Polypropylene and Other Fibers," *Journal of Textile Institute*, 81(2), p. 135-141, 1990.

11. Olivieri, P., Brachesi, M. and Ricupero, T., "Thermal Bonding-The Fastest Growing Application for Polypropylene Staple: Success and Development," Polypropylene Fibers and Textiles, 4th International Conference on Polypropylene Fibers and Textiles, Plastics and Rubber Institute, Nottingham, U.K., p.40/1-40/10, 1987.

12. Schutz, J., Bechter, D., Maag, E. and Kurz, G., "Thermobonding of Nonwovens," *Textil Praxis International*, 46, p.1236-1240, November, 1991.

13. Warner, S.B., "Thermal Bonding of Polypropylene Fibers," *Textile Research Journal*, 59, p.151-1559, 1989.[13]

14. Whitwell, J.C. and Fraser, W.A., "Infrared Laser Bonding of Thermoplastic Monofilaments," *Textile Research Journal*, 41, p. 1003-1005, 1971.[14]

15. Wu, Z., H. Davis and S.K. Batra, "Correct Ray-tracing Analysis for Interference Microscopy of Fibers," Proceedings of the Royal Society, London, A450, p. 23-36, 1995.[15] ***— INJ***

Multipass Beta Filtration Testing For the 21st Century

By John G. Eleftherakis and Abraham Khalil,
Fluid Technologies, Inc./SPX Filtran, Stillwater, Oklahoma

Abstract

The current ISO 4572 Multipass Filter Test Procedure has not been substantially revised since its approval as an ISO document in 1981. However, proposed revisions will likely be adopted shortly which will have far-reaching impact in liquid multipass filter testing and for virtually all industrial applications. These revisions include the adoption of a new test dust to replace the discontinued AC Fine Test Dust (ACFTD), a revised particle counter calibration procedure using National Institute of Standards & Technology (NIST) traceable calibration fluid, a new on-line particle counter, sample delivery and dilution system validation procedure, and a new reporting format. These changes result in a new definition for assessing and rating filter performance.

This paper discusses these changes in detail and the resulting impact on the filtration industry. For example, the most significant revision pertains to use of a revised ISO 4402 standard for calibration of liquid particle counters. Until now, particle counter calibration fluid containing ACFTD was used to calibrate particle counters. This test dust is no longer manufactured due, in part, to the inability of the manufacturer to produce a consistent particle distribution of ACFTD from one batch to another. This inconsistency in the test dust, and also in much of the calibration fluid containing the test dust, created a great challenge for labs to correlate particle count results and filter test data.

The revised ISO 4402 calibration standard will require the use of a new NIST Standard Reference Material (SRM) calibration fluid using a new test dust called ISO Medium dust, which has virtually replaced ACFTD. This new test dust and the calibration fluid containing it is much more consistent and reliable, allowing for better correlation of results.

The analysis conducted by NIST to certify the calibration fluid as a SRM found what before was defined as a 2 micron particle was actually a 4.6 micron particle and what was defined as a 15 micron particle was actually a 13.6 micron particle. This finding will redefine liquid filter performance information based on particle counts to the effect that, in general, fine filters will appear less efficient than previously reported and coarse filters will appear more efficient.

While other revisions to ISO 4572 will have less impact, they are presented. Filter test engineers, filter users and manufacturers, and filter sales personnel will benefit by educating themselves now on the impact of these revisions in order to best serve the filtration industry and filter users.

Introduction

The Beta Ratio derived from the multipass test method for liquid filters has become a primary means of rating the particle separation efficiency and contaminant removal capability of a liquid filter at a single particle size. [1] This rating originates from a preceding test standard to ISO 4572 (1981) [2] called the OSU-F-2 test. [3] By definition, the Beta Ratio (or filtration ratio as used in ISO 4572) of a filter at a specific particle size is "the ratio of the number of particles greater than a given size (µm) in the influent fluid to the number of particles greater than the same size (µm) in the effluent fluid." [2]

Determining the Beta Ratio of a filter is a matter of precise control of test materials and conditions described in the ISO 4572 test standard. One can expect that if test materials and test conditions change, so will the Beta Ratio of a filter. Change in Beta Ratios is exactly what will happen with changes proposed in the test conditions to the ISO 4572 test standard as documented in ISO/DIS 4572. This standard will become ISO 16889 when approved. [4]

Recent technological developments in the areas of contaminant description, particle counter calibration and automation of test equipment compelled changes to the ISO 4572 test standard. The most significant of these developments is a coming change in the particle counter calibration procedure used to calibrate the liquid particle counters for use in the ISO 4572 filter test procedure. This calibration procedure is ISO 4402. [5] A new calibration fluid has been developed

and will be a National Institute of Standards and Technology (NIST) traceable, Standard Reference Material (SRM). This and other changes will result in a more accurate and repeatable test method even though the changes may produce confusion and frustration in the filter industry during a short transition period.

It is the authors' hope that this paper will help justify the changes and ease the transformation from a good filter test standard to a better filter test standard. The proposed changes are presented in the following sections on test materials, test equipment, and data collection and reporting.

Proposed Changes of Test Materials

Following are proposed changes to the test materials used in the ISO 4572 test procedure.

Test Dust

One source of variability with multipass test data in the past was with the test dust, ACFTD. This test dust was specified for use in ISO 4572 and the OSU-F-2 test since the early 1970's. The use of this test dust has been a long-standing topic of discussion at the various industry standards committees overseeing filtration test standards. The variability in the particle size distribution of ACFTD from batch to batch below 10 microns was reported to be most variable. The manufacturer, in fact, decided to discontinue its test dust manufacturing operations, including the manufacturing of ACFTD, partially as a result of its inability to control dust consistency.

With ACFTD no longer manufactured and the industry stock piles dwindling, the National Fluid Power Association (NFPA) committee on contamination, NFPA T2.9, adopted a commercially available replacement test dust. This dust has been internationally accepted, and is an international standard which standardized the supplier's manufacturing process. [6] The new test dust called "ISO Medium" is similar to ACFTD in that it is a silica material. [7] The particle size distribution, compared with ACFTD, is shown in *Table 1*.

Table 1
ISO MEDIUM VS. ACFTD

Particles per ml greater than indicated particle size (1 mg/L suspension)

	ACFTD	ISOMTD (SAE 5-80)
1 µm	1750	1940
2 µm	1400	1650
3 µm	992	1290
5 µm	517	758
7 µm	294	465
10 µm	144	215
12 µm	95.4	127
15 µm	55.2	67.6
20 µm	25.5	29.4
30 µm	7.50	7.69
40 µm	2.87	2.53

Note: The particle counts shown in *Table 1* were generated from particle counters calibrated to ISO 4402 using ACFTD (Batch 169) suspended at 5 mg/L in MIL-H-5606 fluid. These particle counts were not generated in accordance with ISO/DIS 4402 [8] calibration procedure discussed below.

As indicated from the particle size distribution comparison in *Table 1*, ISO Medium has slightly more particles at 1 mg/L concentration, particularly below 20 microns. The number of particles at and greater than 20 microns is about the same as ACFTD. What this means from a filter test standpoint is that filters will be challenged with more smaller particles with ISO Medium than with ACFTD. Differences in filter test data have generally shown the same efficiency of particle removal as compared to ACFTD but higher capacity for liquid filters, but the reverse has also been known to occur.

Calibration Fluid

ISO 4572 requires calibration of particle counters per ISO 4402. [5] Accurate and consistent calibration directly impacts Beta Ratios. With ACFTD no longer available, ISO 4402 will also be changed to require the use of ISO Medium dust for calibration fluid.

Most laser-light particle counters size particles by reading a millivolt level of light reflected or blocked from a particle passing between a light source and the sensor of the counter. Particle counters are calibrated by passing a sample of calibration fluid containing a contaminant, such as dust or latex spheres, having a "known" particle size and/or count. As the calibration fluid is passed between the light source and sensor, the counter is adjusted to read the particle sizes and number of particles greater than those sizes based upon the "known" distribution and concentration. Once calibrated, the counter can then be used to generate particle counts for the upstream and downstream samples from the multipass filter test, resulting in a Beta Ratio for all particle sizes counted.

The analysis performed on ACFTD years ago to determine its "known" distribution was based upon microscopic particle counting. While microscopic particle counting was the best technology available at the time, more advanced analyses with greater accuracy are now available.

With the variability of ACFTD resulting in Beta Ratio variability, the NFPA T2.9 committee recognized that the adoption of a new calibration fluid standard was an opportunity to also improve the particle counter calibration procedure. The objective was to develop an NIST traceable, SRM for the calibration fluid. The project was proposed and accepted by NIST, and Fluid Technologies, Inc. (FTI), an SPX Filtran business, was chosen as the sole supplier of the test dust in oil suspension that would become the NIST SRM.

With the advanced particle measurement technology available at NIST and the contaminant handling and analysis expertise available at FTI, an extensive analysis effort was

performed to better define ACFTD and ISO Medium particle sizes. By using advanced particle counting techniques such as electron microscopy, image analysis, and optical particle counting, NIST found:

1) The ACFTD particle size distribution is not accurately defined by microscopic analysis;

2) Light-based particle counters were not set to read particle sizes accurately due to the inaccuracy of the microscopic counts of ACFTD; and

3) The calibration fluid produced by FTI using ISO Medium dust will qualify as an SRM with a coefficient of variance less than 2% for less than 10 micron particles and 6% across the full particle size range for a batch of 300, 500 milliliter bottles. (SRM 2806 is the NIST reference number assigned to the fluid.) [9]

Table 2 provides a general correlation between the ACFTD particle sizes and the new proposed ISO/DIS 4402 particle sizes based on ISO Medium dust and the NIST analysis. (The reader should note that at the time of publication, the data in *Table 2* was correct. NIST may update these numbers by the time the SRM is available for purchase.) [10]

Table 2 shows that what was defined as, for example, a 2 µm particle of ACFTD was and always has been a 4.6 µm particle, and what was defined as a 15 µm particle was, in fact, a 13.6 µm particle.

The impact this analysis will have on filter Beta Ratios is generally understood. First, since 2 µm was the smallest particle most light-blockage counters claimed to measure in oil based on an ACFTD calibration, the smallest particle they will be able to read with an ISO Medium calibration is 4.6 µm. Light-scattering counters generally have a lower noise level threshold and will likely be able to read sizes smaller than 4.6 µm. In any event, filter Beta Ratios below the redefined particle size limits of a particular counter technology will not be possible unless there are advancements in particle counter technology.

Second, fine filters (approximately 10 µm filters and below) will appear less efficient than before and coarser filters (above 10 µm) will appear more efficient. NOTE: There is no change in actual filter performance, only particle size definitions have changed. *Figure 1* plots one company's apparent Beta Ratio and Efficiency vs. Particle Size correlation between the ACFTD distribution and the ISO Medium distribution based on the NIST analysis for three types of filters.

Table 2
CONVERTING OLD ACFTD SIZES
TO NEW NIST SIZES

ACFTD Size, µm	New NIST Size, µm
1	4.2
2	4.6
3	5.1
5	6.4
7	7.7
10	9.8
15	13.6
20	17.5
25	21.2
30	24.9
40	31.7

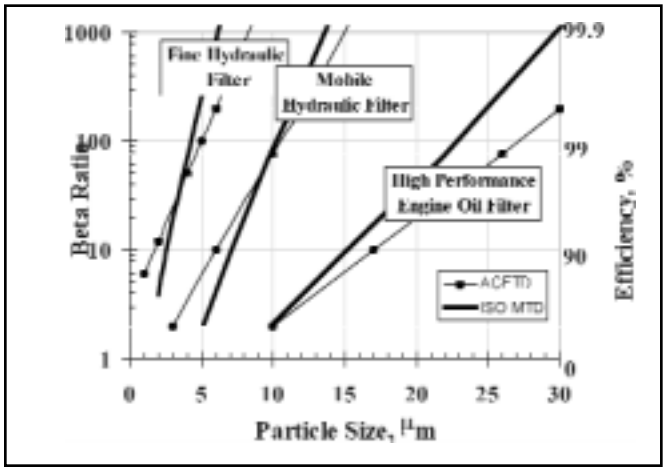

Figure 1
ONE COMPANY'S APPARENT PARTICLE REMOVAL CHARACTERISTICS OF THREE TYPES OF FILTERS AS EXPECTED USING THE ACFTD AND NEW NIST CALIBRATION METHODS [10]

Note: The NIST plots in *Figure 1* are theoretical plots based upon the expected data shift resulting from the new ISO/DIS 4402 [8] calibration and are not based upon actual test data.

Antistatic Additive

Another source of multipass test variability has been the build-up of static electricity in test systems. A debate exists as to how to avoid the effects of static build-up on filter performance. One thought is to add an antistatic additive to the test fluid. An opposing thought is to control lab conditions and fluid condition to minimize static build-up. As a compromise between the two positions, a revision to ISO 4572 is proposed to simply recommend the conductivity of the test fluid be measured and maintained within a range of 1,000 to 10,000 pS/m. A notation is made that test results may be effected if an antistatic additive is used. [4]

Other subtle changes to test materials and their handling are proposed in ISO/DIS 4572 and the reader is encouraged to review it further.

Proposed Changes Of Test Equipment

Following are proposed changes to the test equipment required.

On-Line Particle Counting Calibration

In the 1981 version of ISO 4572, test fluid sampling to obtain the upstream and downstream particle counts was allowed to be accomplished by either on-line sampling with the particle count analysis also performed on-line or bottle

Figure 2
AUTOMATED MULTIPASS FILTER/MEDIA TEST STAND WITH AN ON-LINE PARTICLE COUNTING SYSTEM

sampling with the particle count analysis conducted independent of the test stand using a counter-top batch particle counter. The bottle sampling method is conducted per ISO 4021 covering the extraction of fluid samples from an operating system and the particle count analysis is conducted per accepted procedures. [11]

The proposed changes to ISO 4572 will not allow the bottle sampling method to be used. Therefore, Multipass Filter Test Stands will require the capability to perform particle counting on-line. There are two primary reasons to justify this change:

1. The variability with particle counts associated with bottle cleanliness, sample extraction and sample preparation are avoided by using on-line counting.

2. The improvement in test automation and particle counting technology in recent years makes on-line particle counting reliable and cost effective *(Figure 2)*.

In addition to these two justifications, some test labs today already use on-line particle counting, and upgrading test systems that don't have on-line particle count capabilities is cost effective.

With the new multipass filter standard, the on-line particle counting system must meet a stringent calibration and validation process standardized by ISO/DIS 11943. [12] Only test stands meeting the yet-to-be approved ISO 11943 requirements will qualify to perform the ISO 4572 test. The requirements of ISO/DIS 11943 can be classified into three distinct efforts.

- First it requires a primary calibration of the particle counter sensors used in the on-line system.
- Second is the validation of the on-line system's ability to maintain controlled contaminant suspension and sample delivery conditions and a secondary calibration of the particle counter sensors.
- Third is the validation of the on-line dilution system if one is used.

Regarding the calibration of the particle counter sensors, primary calibration is performed to the ISO/DIS 4402 requirements discussed above. When two sensors are used in the system (one upstream and one downstream), a primary calibration is to be conducted on both sensors upon installation of new sensors, upon major service of the system, or at the manufacture's recommended calibration frequency.

Between primary calibrations, secondary calibrations are required after each primary calibration and at least every three months or when particle count discrepancies occur. The secondary calibration is required only on one sensor if two are used and both have had a primary calibration. The second sensor is then matched to the other. This is performed in conjunction with the validation of the on-line sample delivery system. [12]

Proposed Changes of Data Collection and Reporting

Following are proposed changes to test data collection and reporting:

Reporting Times

With the automation of test systems and particle counters, it is now possible to collect data continuously (as frequently as every 30 seconds with test equipment manufactured by at least one manufacturer) and select from a data file only that data that is of interest. In the current ISO 4572 standard, data is reported at five points during the test at which either a stated time has elapsed or a predetermined pressure drop point is reached. For instance, data is to be reported at 20% and 80% of the terminal pressure drop. The typical time it takes to go from 0% to 20% is much longer of a time than it takes to go from 80% to 100%, even though both ranges cover only 20% of the terminal pressure drop. This time inequality results in a significant amount of data taken but not reflected in the final Beta Ratios of a filter.

To address this, a change is included to collect data throughout the test and report at 10 equal time intervals based on total test time (e.g., every 10 minutes for a 100 minute test, or every six minutes for a 60 minute test, etc.). The particle count data presented at each interval is the average of all particle counts taken between the intervals. This approach gives equal weight to data taken throughout the test. This will also mean that a Beta Ratio at a particular size will be determined by using data from 10 equal points during the test rather than five predetermined points and, thus, will be based on more data. [4]

Conclusion

The Beta Ratio for a liquid filter determined by the ISO 4572 Multipass Filter Test Method has became the international standard for determining the contaminant removal characteristics of a liquid filter. Literally thousands if not hundreds of thousands of these tests are performed annually worldwide. Filter purchasing decisions are often made after considering the Beta Ratio test data. Thus, changes made to the ISO 4572 test standard will have far-reaching impact on the filtration industry. Filter manufactures and users will benefit by becoming knowledgeable of the proposed changes to ISO 4572.

The most important and far reaching of the proposed changes involve the test dust used in the test and the use of a new, NIST Standard Reference Material calibration fluid for calibrating particle counters used for the test. The combination of these and other changes will result in more accurate, repeatable test data. Test data on fine filters (10 µm and below) will generally show those filters to be less efficient and coarser filters (above 10 µm) will appear more efficient. In reality, however, the filters are performing the same but the particle size data is more precisely represented.

Understanding these changes will be critical to easing the

transition from the current ISO 4572 test standard to the ISO/DIS 4572 once the revisions are formally approved. Such approval may be several months away if not one year or more, but the benefits resulting from the revisions will improve the ISO 4572 test standard significantly. Filter manufactures and users will benefit by learning of the revisions and the impact on the industry to ease the transition.

References:

1. Eleftherakis, John G. "Advanced Filter Test Methods – Utilizing the Multipass Test," Nonwovens Conference, TAPPI Press, Atlanta, GA (1993)

2. ISO 4572, "Hydraulic Fluid Power - Filters – Multipass Method for Evaluating Filtration Performance," Annex, International Organization for Standardization, Stockholm, Sweden (1981).

3. OSU-F-2, "Multi-pass Method for Evaluating the Filtration Performance of Fine Hydraulic Fluid Power Filter Element," Recommended Procedures for Evaluating Fluid Power Components and Systems, Fluid Power Research Center, Oklahoma State University, Stillwater, Oklahoma, FPRC No. 72-1, Pgs. 21-33 (March 1972)

4. ISO/DIS 4572, "Hydraulic Fluid Power-Filters-Multipass Method for Evaluating Filtration Performance of a Filter Element," International Organization for Standardization, Stockholm, Sweden (Sept. 97).

5. ISO 4402, "Hydraulic Fluid Power – Calibration of Liquid Automatic Particle Count Instruments – Method Using Air Cleaner Fine Test Dust Contaminant," International Organization for Standardization, Stockholm, Sweden (1977).

6. ISO/FDIS 12103-1, "Road Vehicles Test Dust for Filter Evaluation, Part 1: Arizona Test Dust," International Organization for Standardization, Stockholm, Sweden (1997).

7. Other names for ISO Medium which have surfaced during its development are SAE Medium, SAE 5-80, PTI Fine, and PTI 5-80. The official name is ISO/FDIS 12103-A3 dust. See Reference 6.

8. ISO/DIS 4402, "Hydraulic Fluid Power – Calibration of Liquid Automatic Particle Counters," International Organization for Standardization, Stockholm, Sweden (Sept. 97).

9. Fletcher, Robert A., et. al., "Development of a Standard Reference Material for the Fluid Power Industry: ISO Medium Dust in Oil," 47th National Conference on Fluid Power, National Fluid Power Association, Milwaukee, WI (1996).

10. Verdegen, Barry, "Changes in Particle Counting and Contamination Control Standards for Hydraulics and Lube Oil Applications," Technical Brief for NFPA T2.9 Contamination Technology Committee (Sept. 1997).

11. Eleftherakis, John G. "A Primer on Particle Counting." Hydraulics and Pneumatics, Penton Publishing, Cleveland, OH pp. 34-36, November 1992.

12. ISO/FDIS 11943, "Hydraulic Fluid Power-On-line liquid automatic particle-counting systems-Methods of calibration and validation," International Organization for Standardization, Stockholm, Sweden (1996).

— INJ

EMERGING TECHNOLOGY WATCH

Wetform Nonwoven Watch

The division between specialty papers and wetform nonwovens is very hazy and indistinct. Consequently, developments in one sector can often be adapted and adopted in the other sector. Some product development problems and goals are often very similar.

A problem that has existed for years in cigarette paper may soon be solved. The number of fires caused by smoldering cigarettes resulted in a call for a cigarette paper that addresses the problem.

A new cigarette paper developed by Philip Morris Companies was being considered for market introduction in several states in the U.S. This cigarette will utilize a paper featuring paper rings or high density zones that act as "speed bumps," causing it to burn more slowly when the lit end crosses over them. It is also reported that the cigarette may extinguish itself when resting in an ashtray and on certain types of fabrics. As a consequence, it is claimed that it goes a long way toward meeting the goal of curbing fires ignited by smoldering cigarettes.

The new product has been named "PaperSelect" and will apparently be featured in one brand of the company's category of premium brands if the marketing trials prove successful.

This feature built into the paper apparently does not reduce the ignition propensity of the cigarette. The company has indicated they might be willing to license the concept to competitors if it proves highly successful. Current capacity is somewhat limited.

* * *

Another area of considerable development in the papermaking/wetform sector is in the recycling and the de-inking of the waste paper. A novel approach to this problem has been made by two different groups wherein waste paper computer printing operations is recycled one sheet at a time. In one case, thermal and mechanical action enhances the release of the ink toner used in laser and similar thermal printing units. This is followed by the addition of a small amount of coating which provides a fresh, white surface. The other system involves adding a coating system to both sides of the paper sheet to give a clean surface on both sides. In the case of both processes, a small desktop unit accomplishes the recycling process.

Research and development efforts on processes for removing ink from paper to permit economic recycling continues. Researchers at the University of Florida have devised an inexpensive blend of chemicals that does a better job for debonding the inks from the paper. This system is claimed to claimed to provide the route to a higher quality of paper than is normally possible with de-inked fiber, and at an economic cost. For more information: Prof. Brij M. Moudgil, Materials Science & Engineering Department, University of Florida, Gainesville, FL; 352-846-1194.

* * *

The *Wall Street Journal* recently reported on a recycling system being used in Russia that sounds very familiar. In this case, a warehouse filled with tons of Russian rubles in the form of worthless paper money has been provided to the Ulyanovsk Roofing Material Factory to produce cellulosic felt stock for the production of coated roofing material. The report indicates that the paper rubles cost less than $15 per ton, about one-third the price of scrap paper.

At least in one portion of Russia, the citizens have roofs covered with money.

Energy Absorber

In numerous applications, textile assemblies are required to absorb an inordinate amount of energy. The more energy that can be absorbed, the better the performance of the fiber assembly.

An automotive seatbelt is a good example. Fibers with better energy-absorbing capabilities could dissipate a greater amount of the energy of a collision that is normally transferred to the wearer of the seatbelt.

A new block copolyester polymer has been developed which the inventors claim have enhanced energy-absorbing properties. The block copolymer comprises poly(ethylene terephthalate) and poly(caprolactone).

The block copolymer is produced by reacting PET with the caprolactone monomer, along with a tin catalyst in a twin-screw extruder. The resulting modified copolyester can then be spun, drawn into filaments, and relaxed in the usual manner to produce a continuous filament; such a material has a high degree of crystalline orientation phase and a large fraction of unoriented amorphous phase.

This combination provides the energy-absorbing feature because of the presence of the strong, stiff crystalline segment alternating with the amorphous, "springy" phase. In this application, the fiber delivers a three-step restrain reaction during a crash. At the moment of impact, the filaments hold occupants in place. Immediately afterward, the filaments stretch enough to limit the force on the occupant. Finally, the ultimate high strength of the filaments helps to prevent impact with dashboard, steering wheel or windshield. Seatbelts made with this fiber are designed for occupants of any size, compared with current safety belts, which are designed for an average car passenger, a 175-pound man.

The manufacturing method suggests that it may be possible to modify an existing polymer with a short, thermo-mechanical maceration step in the presence of a suitable monomer and catalyst prior to extrusion. This may afford an economic way to produce a spunbond fabric with useful elasticity. (For more

information see W. Tang, et al., *J. Appl. Polym. Sci.*, 74, pp 1858-1867 {1999}).

Glow Discharge Plasma Use

One of the difficult environmental problems particularly prevalent in developed countries is the task of cleaning up "dirty" water, to eliminate hazardous chemicals and drugs polluting much of the water supply. This problem has been exasperated by such factors as pollution of watersheds by the gasoline additive methyl tertiary butyl ether (MTBE) leaking into ground water. Also, recent research has shown that 50 to 90% of pharmaceutical drugs, such as cholesterol inhibitors and estrogen, pass through the body into wastewater systems and then the survive through treatment plants in their active form.

Conventional treatment technologies that have been used, such as biological treatment, do not destroy much of the difficult materials that may show up in wastewater and groundwater.

A new technique developed by Pacific Northwest National Laboratory (PNNL) in Richmond, Washington shows promise for destroying such recalcitrant organic contaminants from water and other pollution systems. Glow Discharge Plasma (GDP) appears to offer hope by itself, or as part of a larger treatment system, to remove contaminants that have proved resistant to traditional methods. This includes such materials as trichlorethylene, chloroform, perchlorethylene, toluene and other materials.

GDP utilizes a strong electric field to accelerate electrons in a non-thermal plasma. Such a plasma is an electrically neutral gas that has very energetic electrons. Contaminated water is continuously circulated in a falling film. As the water circulates, the fast moving electrons in the plasma collide with molecules in the gas above the water and on the water surface. This activity causes the molecules to break apart, forming reactive radicals and ions that react with the surface of the contaminated water, chemically destroying the contamination.

The key to GDP's versatility is that the non-thermal plasma creates both oxidizing and reducing active species and they can be controlled to address almost any contaminant, according to PNNL personnel. Further, this treatment method holds promise for treating other surfaces, such as fabric polymeric surfaces, to achieve chemical modification. Further details can be obtained at the PNNL website (www.pnl.gov/breakthroughs).

This treatment technique is somewhat reminiscent of research work carried out at North Carolina State University on non-aqueous fiber preparation and finishing. This work compared various vacuum plasma processes, both inductive and capacitive, to atmospheric plasma processes. The latest work on this project has involved treatment of woven fabric under vacuum plasma processes, in the presence of fluorochemical gases to render the fabric more hydrophobic. This treatment apparently can follow multiple reaction paths, which can involve film-forming modes as well as chemical scarification of fiber surfaces leading to increased chemical reactivity. ***— INJ***

Hepatitis-C Concern and Nonwovens

Because nonwoven fabrics are widely used in an array of medical products, the barrier properties of such nonwovens have been studied extensively.

Such barrier properties have become of even greater importance as the shift in medical product priority has moved in the past few years from User Comfort and Cost to User and Patient Protection.

In this paradigm shift, the variety of hazards faced by medical professionals has comprised a fairly extensive list of pathogens and accompanying diseases. Apparently Hepatitis-B is no longer much of a threat to medical professionals, as an excellent vaccine exists and the current policy is to use it judiciously and promptly. Similarly, Hepatitis-A & D are under good control, with appropriate standards of medical practices.

HIV, which has certainly received a great deal of publicity, is a rather limited transmission risk. Apparently there have been over 500 HIV-positive exposures in the past 15 years, but with a minimum number of transmission cases.

Malaria, babesiosis, borreliosis, erlichiosis and syphilis are some diseases that occasionally may present a bloodborne exposure transmission risk. In case of these latter pathogens, a relatively large volume of blood is involved in the exposure until pathogenic transmission occurs. Other problems are uncommon in the developed nations and hence of much less concern.

The good control of these bloodborne pathogens is no reason to relax, however, as Hepatitis-C is still of major concern associated with blood exposure. Such concern is warranted, as Hepatitis-C is a killer; about 10,000 people die of the disease each year and the death toll is rising. It has infected four times as many people as has HIV. At least four million Americans have it — 2% of the population. Many Americans infected with Hepatitis-C are unaware they have the disease.

What makes Hepatitis-C difficult to manage is the fact that it can lurk within the human body unawares. People seldom get sick when first affected with the virus, unlike what happens with its cousins Hepatitis-A & B. Instead, the microbe quietly damages the liver for 20 years before symptoms may emerge. Because of this, officials at the Federal Center for Disease Control and Prevention predict that in the next 10 years the Hepatitis-C death toll will triple, eclipsing that of AIDS.

The difficulty in dealing with Hepatitis-C is the fact that the protein coating of the virus constantly mutates. As a result, when a vaccine is developed that primes the body immune cells to recognize the intruder, it is effective for only a short period time.

All of this proclaims that the nonwovens research devoted to medical barrier performance must be continued at an aggressive level.

NONWOVEN PATENT REVIEW

Intellectual Property and Technology Transfer

Obtaining an issued U.S. patent can be an expensive exercise. Typically, the cost can run from a few thousand dollars to hundreds of thousands of dollars. And that is not the end: to keep a patent valid, regular fees are required to be paid. Clearly, obtaining and maintaining a patent is a costly affair. This expense exists even though it is estimated that most corporations use only about 3% of the patents they have obtained.

And what if a company finds that it really doesn't need or use the patent? Perhaps a better solution to the problem or an alternate process has been developed. Can the cost incurred be recovered?

Such a financial recovery from the U.S. Patent and Trade Mark Office is definitely not possible. However, if another company can be found that can use the technology, suddenly an unused patent can become valuable.

Many companies in the United States and elsewhere are beginning to pursue this approach, by licensing or selling unused technology. Although there is no guarantee of success in this approach, enough companies have converted unused intellectual property into cash to make the strategy very attractive. The activity has become so profitable that many corporations are installing "intellectual-asset managers," modifying their patent strategies, conducting patent audits, and using various other management and sales techniques to foster the activity.

As might be expected, use of the Internet has also been extended to this activity as well. Probably the best known example is yet2.com, an Internet site established by a former DuPont global-development manager for their Lycra elastomeric filament business.

Yet2.com bills itself as a site for exchange of intellectual property, serving both the buyer and the seller of technology. Just recently they announced the addition of 12 new partners to their listing of companies interesting in licensing technology. These new additions (including Bayer, NEC Corporation and Sumitomo Chemicals) joined 35 other companies, including BASF, Battelle, 3M Company, Arthur D. Little, Dow Chemical, DuPont, Mitsui Chemical and Monsanto. The company has already established offices in London and Tokyo to augment its headquarters in Cambridge, Massachusetts.

Yet2.com (www.yet2.com) gives these companies, and their other subscribers across many industries and R&D interests, a vehicle to announce and market technologies they have developed, but are willing to let others fully exploit.

Will this type of e-business be successful? It is a little early to know, but already several others are entering the arena, including Patent & License Exchange, Intellectual Property License Exchange (www.iplx.com), The Intellectual Property Network (www.ipnetwork.com), Licensing Executive Society International (www.lesi.org), Tech Exchange (www.techexchange.com) and others.

RECENT PATENTS

Hydroentangled Pulp/Spunbond

A lightweight spunbond fabric (20 gsm or less) is combined with a lightweight woodpulp tissue (20 gsm or more) and the combination is subjected to high pressure waterjet entanglement. The web is then creped, either wet or dry, using a formula for determining the Compression Factor for creping.

The creping is conducted to provide both MD and CD elongations of 50% or more up to 100% after treatment. This process is claimed to give an economic wiping fabric with good fabric strength and balanced orientation.

U.S. 6,080,466 (June 27, 2000); filed November 12, 1997. "Composite sheets for wiping cloths." Assignee: Nippon Paper Industries. Inventors: Jiro Yoshimura, Akira Sakamoto, Hirotoshi Aikawa, Yoichi Yamazaki.

Multiple Layer Wiping Article

A disposable wiping article is disclosed, produced from a nonwoven fabric having at least two layers. The first layer has a wet extensibility greater than that of the second layer. The first layer can be an apertured, dry creped web of cellulosic fibers and the second layer can be a nonwoven web comprising synthetic fibers.

The two layers are bonded together with an intermittent pattern, which bonding inhibits extension of the first layer when the fabric is wetted and the cellulosic fibers swell. Because of this inhibition, the first layer undergoes buckling or puckering in the Z-direction upon wetting, which results in a bulky wiping fabric.

The claims also include the wiping fabric with the addition of soap, a lathering agent or a cleansing agent.

U.S. 6,060,149 (May 9, 2000); filed January 26, 1998. "Multiple layer wiping article." Assignee: The Procter & Gamble Company. Inventor: Nicholas James Nissing, David Michael McAtee, David William Cabell.

A Composite Elastic Material

A composite elastic material is described which comprises a nonwo-

ven fabric secured to an elastic member. The nonwoven fabric is preferably a carded polyester web with a small amount of bicomponent binder fiber, subjected to waterjet entangling to provide a MD/CD elongation ratio of 1:4 and a basis weight of 20 gsm. The elastic member is preferably an elastic film having a thickness of 40 microns.

The film is extruded from a compound comprising 80 parts of an isoprene or a styrene-butadiene synthetic rubber and 20 parts of ethylene-vinyl acetate copolymer. The elastic film has an elastic recovery of about 60% or more and a breaking elongation of about 200% or more.

The elastic film and the nonwoven fabric are bonded together at a plurality of points in the stretchable direction of the nonwoven fabric. The composite nonwoven fabric is heated and drawn at the softening point temperature of the thermoplastic bonding component.

The composite elastic material has multiple-stage elongation characteristics, including a first stress lowering point caused by changes in the structure of the nonwoven fabric (rupture of secondary bonds) and a second stress lowering point occurring at an elongation greater than the first stress lowering point; the second stress lowering point is caused by breakdown of the elastic member.

The composite elastic material can be used as an elastic component in sanitary articles, such as baby and adult diapers and a sleeve portion of a medical gown.

U.S. 6,069,097 (May 30, 2000); filed September 16, 1997. "Composite elastic material having multistage elongation characteristics and method of manufacturing the same." Assignee: Paragon Trade Brands Inc. Inventors: Migaku Suzuki, Hiroaki Fukui.

A Drum for Hydraulic Needling

The permeable drum disclosed in this patent is used for hydraulic needling of nonwovens, tissues or other permeable materials. The drum consists of a normally perforated sheet metal drum onto which strips that are thin and extend axially over the length of the drum are arranged with small distances between them around the drum. The strips radially support a very thin sheet metal jacket with microfine perforations. This produces a uniform flow of liquid through the material that rests upon the jacket.

The strips can be joined together, for example, to form a honeycomb profile and thus uniformly transfer the hydrodynamic load encountered during needling to the screen drum.

U.S. 6,055,710 (May 2, 2000); filed November 10, 1997. "Device for hydraulic needling of fleeces, tissues or the like." Assignee: Fleissner GmbH & Company Maschinenfabrik. Inventor: Gerold Fleissner.

Composite Nonwoven Barrier

This patent discloses a composite nonwoven material suitable for use as a barrier layer or backsheet in hygienic absorbent products, such as disposable diapers, training pants, sanitary napkins, panty shields and adult incontinent products.

The composite nonwoven comprises a nonwoven layer and a microporous polymeric foam layer. The two layers can be joined by coating the foam layer on the nonwoven fabric layer.

The polymeric foam layer has a desired degree of water-impermeability, coupled with a desired degree of air-permeability. The polymeric foam-coated, composite nonwoven is also suitable for use as a barrier layer in the building or construction industry, such as an under-roof layer.

EP1 010 801 A2 (June 21, 2000); filed March 7, 2000. "Composite nonwoven material." Assignee: FiberVisions A/S. Inventor: Erik Neilsen Knud.

Stretch Spunlace with Foam Layer

A method for producing an elastic fabric with multi-directional stretch properties via the spunlace process is disclosed. The laminate is comprised of at least two layers, one layer being a staple fiber web and the second being a foam layer. The foam layer can be an open or closed cell foam.

The two layers are entangled by high pressure waterjets under conditions and to the extent that effective entangling of the fibers within the foam structure is accomplished, without appreciable degradation of the foam structure.

A superior elastomeric fabric with multi-directional stretch properties results from this process. Such a product has many applications in hygiene products, medical products, industrial products, consumer products and others.

U.S. 6,074,966 (June 13, 2000); filed September 9, 1997. "Nonwoven fabric composite having multi-direction stretch properties utilizing a cellular or foam layer." Assignee: None. Inventor: Frank P. Zlatkus.

Plexifilamentary Film-Fibril Web

This invention relates to improved nonwoven sheet products made from highly oriented plexifilamentary film-fiber webs. Such webs are usually produced by flash spinning of a polyolefin solution.

The improved sheet products have high opacity and strength with a much wider range of porosity, or Gurley-Hill porosity values. In particular, the sheet products made with the present invention have considerably higher Gurley-Hill porosity values than similar weight sheet products subject to the same finishing treatments. Also, the nonwoven sheet products can be made which have much lower Gurley-Hill porosity values than prior sheet materials.

The inventors include numerous methods and data characterizing the webs and sheets that form the improved sheet materials. They claim these materials are particularly useful in medical applications.

U.S. 6,070,635 (June 6, 2000); filed April 17, 1998. "Nonwoven sheet products made from plexifilamentary film fibril webs." Assignee: E. I. du Pont de Nemours and Company. Inventors: Ralph A. Franke, Hyun S. Lim, Michael P. Malone, R. Gail Raty, Akhilswarg Vaidyanathan. ***— INJ***

At The Center Of Nonwovens

The University of Tennessee's TANDEC helps create a place where academics and the nonwovens industry can meet

In 1983, a partnership was formed between The University of Tennessee (UT), Knoxville, TN, and Exxon Chemical in the area of melt blown technology due to a proposal submitted by a member of UT, Dr. Larry Wadsworth. Six years later, this partnership was expanded to become The Textiles and Nonwovens Development Center (TANDEC) located right at UT. Today, TANDEC strives to provide a higher level of service to the nonwovens industry through expanded technology expertise, industry-wide annual courses and a corporate membership of more than 20.

According to Dr. Wadsworth — who currently acts in the capacity of professor and senior executive, technology and marketing for TANDEC — the center has continued its work with melt blown technology through the pilot equipment it had received from Exxon in 1983. At the same time, the center has expanded its research and testing offerings throughout the past few years and currently houses six lines, including a one-meter Reicofil 2 spunbond line, a 20-inch Accuweb melt blown line and a six-inch melt blown line. Additionally, TANDEC contains a 24-inch Reicofil melt blowing line with bi-component technology, a 12-inch JML hot melt adhesive laminating line and a 24-inch Ramisch Kleinweifers calender with five rolls. The center also houses additional equipment, such as a carding machine, a coater/laminator/oven, a foam finishing pilot line, a heat-and-stretch pilot line and Corona Treating equipment.

In addition, in 1997 TANDEC renewed its agreement with Exxon, which in turn transferred its melt blown technology to TANDEC Technology Licensing (TTL), a licensing division of the UT Research Corporation. "There was a need for a neutral, university-based laboratory to develop a more fundamental understanding of melt blowing technology, develop new products and evaluate new resins on industrial-scale equipment," Dr. Wadsworth explained.

In addition to the spunbond equipment, in 1989 there was a extension of the melt blown program, making industry-standard spunbond pilot equipment even more available to companies that could either sponsor research or obtain use of the melt blown and spunbond equipment for a daily fee. "The companies benefit from the expertise of our scientists and well-trained technicians without having to operate expensive pilot lines at their facilities," Dr. Wadsworth stated. "Even producers that have spunbond and melt blown pilot lines often prefer to work with resin producers or customers at TANDEC to evaluate resins and to develop web products at the more neutral university setting."

TANDEC has continued to work towards its primary goal of creating an environment for ongoing innovation that also guarantees the protection of proprietary and confidential information of members and clients. Says Dr. Wadsworth, "Each client's research and pilot line trials are treated discreetly and independently and the entire TANDEC staff is sensitive to the absolute boundaries of information flow. Through this focused effort, we strive to maintain a neutral development site that can be confidently and effectively used by all members and clients."

Due to its neutral nature, there are a good number of projects underway at TANDEC from a variety of clients. One such project is a three-year undertaking jointly funded by UT and Reifenhauser to demonstrate the successful production of side-by-side bicomponent (bico) fiber melt blown nonwovens on the first prototype bico melt blown line that Reifenhauser has manufactured, which is housed at TANDEC. "We are working to maximize the amount of information that can be obtained about the effect of processing conditions and die geometry on the properties of mono and bico melt blown fiber webs and to optimize these processing conditions," Dr. Wadsworth explained. Other projects at TANDEC include the fabrication of nonwovens from cotton/biodegradable binder fibers, image analysis of fibers and webs and flame retardant melt blown webs.

Research and testing are not the only services TANDEC provides for both the academic and professional members of the nonwovens industry. Through the TTL division of the UT Research Corporation (UTRC) — which bought Exxon's melt blown licensing business in 1997 and has the primary assets to 19 active patents in melt blowing and related technologies, associated copyright interests and 37 active melt blowing licenses — the Center is able to license out the transferred technologies and other nonwoven process and application intellectual property developed by TANDEC. One such TANDEC development is "Tantret" electrostatic charging technology that was invented by

Some of the action from a past TANDEC Nonwovens Conference. The 10th annual event is set for November 7-10 at The University of Tennessee-Knoxville.

Dr. Peter Tsai and Dr. Wadsworth. The technology utilizes novel DC corona electrode designs and arrangements that electrostatically charges dielectric nonwoven webs or composites either in-line during production or off-line after web production.

Throughout the past 16 years, TANDEC has continued to keep its well-known position within the nonwovens industry through making itself accessible in a number of ways. Not only has the center worked to maintain and upgrade its melt blown, spunbond and thermal calendering equipment for research and use by the industry, it has also offered an annual nonwovens conference since 1990 *(see sidebar)*. "The annual TANDEC Nonwovens Conference has been well attended by the industry and has obtained an international reputation as a leading nonwovens conference," Dr. Wadsworth said. Additionally, TANDEC provides tailor-made short courses and hands-on training on its pilot equipment, as well as presents papers at major nonwovens conferences and publishes the results of its processing studies and fiber and fabric characterization work in industry periodicals and journals.

For the future, TANDEC plans to continue to upgrade its existing pilot equipment but does not have any immediate plans to expand. "We will continue to upgrade the pilot lines so that they are representative of widely available commercial equipment," Dr. Wadsworth explained. "Other possibilities include installing bicomponent spunbond capability or in-line SM production." At the same time, the Center will continue to actively develop composites, such as SM and SMS laminates, as the nonwovens industry goes through its different phases of product innovation. ***— INJ***

10th Annual International TANDEC Nonwovens Conference

TANDEC will host the 10th annual International TANDEC Nonwovens Conference from November 7-10 at The University of Tennessee (UT) in Knoxville. The conference is scheduled to include a broad selection of industry speakers and will be attended by professionals in nonwovens, R&D, marketing, production, academic and management.

The conference was started in 1990 as a way of combining two other seminars — a bi-yearly melt blown technology update and an annual nonwovens workshop. Through the years, emphasis has grown to include developments in the areas of spunbond, thermal bond and composite technologies in addition to melt blown technology coverage. In addition to a number of presentations by speakers both from UT and outside the institution, attendees will be able to take part in a poster session and tour the TANDEC facilities.

For more information on attending the 10th annual TANDEC Nonwovens Conference: TANDEC, 1321 White Ave., Knoxville, TN 37996-1950; 423-974-3573; tancon@utkux.utk.edu; web.utk.edu/~tancon/about.html.

The TAPPI Nonwovens Page

Division Presenting Major Awards At INTC

Royall Broughton To Receive TAPPI Technical Award

Royall M. Broughton, Jr., Philpott-Westpoint Steven Professor of Textile Engineering at Auburn University, will be presented with the 2000 TAPPI Nonwovens Division Technical Award and Mark Hollingsworth Prize at the International Nonwovens Technical Conference in Dallas, TX.

A TAPPI member since 1969, Broughton has been an active part of the Nonwovens Division. He has served on the Nonwovens Fibers Committee for many years, and has served as its chairman. He subsequently served as Nonwovens Division Continuing Education Chairman and on the Division Steering Committee.

Albert Hoyle To Receive Leadership & Service Award

Albert Hoyle, president of Hoyle Associates in Alpine, TX, will receive the 2000 TAPPI Nonwovens Division Leadership & Service Award during INTC in Dallas. This award is presented each year to a nonwovens professional who has exhibited outstanding leadership and service to TAPPI, its committees, and the industry.

A TAPPI member since 1974, Hoyle has been involved with the Nonwovens Division since its inception in 1983 and he has served as Division Chairman. Hoyle is also a published author and for a number of years was the author of "Patent Analysis" in the *International Nonwovens Journal.*

Other TAPPI Awards

Certificates of Appreciation

Girish Grover; Program Co-Chairman
James R. Tanger, Nonwovens Binders and Additives Committee Chairman
Michael R. Nijakowski, Properties and Performance Committee Chairman
Joginder S. Malik, Nonwovens Filtration Media Committee Chairman
I. Marshall Hutten, Nonwovens Fibers Committee

Scholarship Award (2000-2001)

Ariana Lyn Birdwell
California State Polytechnic University

Best Paper Awards (1999 Conference)

Michele F. Mlyner, Rohm and Haas
Daojie Dong, Owens Corning Science
Mel Mitchell, Eastman Chemical
Cliff Marshall, Bandz Inc.
Irwin M. Hutten, Hollingsworth & Vose
Stephen Michielsen, Georgia Tech
Aniruddah Mitra, Bhuvenesh C. Goswami, and Maria Cybulska, Clemson University

TAPPI Committee Schedule for INTC

Building and Industrial Mat Committee

Tuesday, September 26; 1:00 - 2:00 p.m.
Topics to be discussed include:

a) Status of EPA Clean Air Ruling
b) Classical Methods T1000-T1005
c) CA Status for Methods T1006-T1017

Fibers Committee

Tuesday, September 26; 1:00 - 2:30 p.m.
Guest speaker presentation by Dr. Larry Wadsworth on TANDEC and its program at the University of Tennessee, Knoxville. Also, Best Paper awardees will be recognized.

Properties and Performance Committee

Wednesday, September 27; 11:00 a.m. to 12:30 p.m.
Mike Nijakowski will report on Committee Action for "Fiber Length Measurement."

Binders & Additives Committee

Wednesday, September 27; 11:00 a.m.-12:30 p.m.
Committee Action for publication of B&A educational materials will be presented by J. Miles. In addition, an "Emulsion Polymer Market Overview" will be presented by P. Wiaczek. Finally, an "Overview of Binders & Additives" technical session will be discussed by M. Alexander.

Process Technology Committee

Wednesday, September 27; 1:00 - 2:30 p.m.
Content of the tutorial given at the November 9 TANDEC meeting will be reviewed.

Filtration Media Committee

Wednesday September 27; 1:00 - 2:30 p.m.
Special guest speaker will be Thad Ptak, who will present an "Overview of Gas Filtration and Filter Testing."

The International Nonwovens Journal is published by INDA, Association of the Nonwoven Fabrics Industry, P.O. Box 1288, Cary, NC 27512; (919) 233-1210; Fax (919) 233-1282; www.inda.org. Sponsored by TAPPI, Technical Association of the Pulp and Paper Industry, P.O. Box 105113, Atlanta, GA 30348; (770) 446-1400; Fax: (770) 446-6947; and ANIC (Asia Nonwoven Fabrics Industry Conference), Soto kanda 6-Chome Bldg. 3Fl, 2-9, Chiyoda-ku, Tokyo 101, Japan; 81-3-5688-4041; Fax: 81-3-5688-4042 The magazine is sent free of charge to INDA, TAPPI and ANIC members.

It's time to recognize some good IDEAs!!!

Announcing the inaugural

IDEA 01

ACHIEVEMENT AWARDS

Co-sponsored by INDA, Association of the Nonwoven Fabrics Industry, and NONWOVENS INDUSTRY magazine.

The IDEA 01 Achievement Awards have been established by INDA and NONWOVENS INDUSTRY *to recognize the members of the nonwovens industry that have contributed the most to the advancement of the business of nonwovens.*

The awards will be presented during IDEA 01, March 27-29, 2001, at the Miami Beach Convention Center, Miami Beach, Florida.

inda

CO-SPONSORED BY

ENTER YOUR NOMINATION FOR THE IDEA 01 ACHIEVEMENT AWARDS IN THE FOLLOWING SEVEN CATEGORIES ...

*** IDEA 01 Equipment Achievement Award ...** Presented to the company with the best equipment new product introduction since IDEA 98.

*** IDEA 01 Roll Goods Achievement Award ...** Presented to the company with the best roll goods new product introduction since IDEA 98.

*** IDEA 01 Raw Material Achievement Award ...** Presented to the company with the best fiber/raw material new product introduction since IDEA 98.

*** IDEA 01 Short-Life Product Achievement Award ...** Presented for the best new short-life product utilizing nonwovens introduced since IDEA 98.

*** IDEA 01 Long-Life Product Achievement Award ...** Presented for the best new long-life product utilizing nonwovens introduced since IDEA 98.

Criteria for the above awards ...

• Market Acceptance, Commercial Viability, Technical Advance and/or New End Use

• New product nominations must have been introduced to the market, either through a technical paper or as a commercial product, since IDEA 98.

• The nominated product must be designed for a nonwoven application or for the production of a nonwoven or in a nonwoven process.

*** IDEA 01 Entrepreneur Achievement Award ....** Presented to the company started since IDEA 98 that has achieved the most since its founding.

* **IDEA 01 Lifetime Achievement Award ...** Presented to the individual or company that has contributed to the advancement of the nonwovens industry for at least 20 years.

To nominate a company or individual follow these three simple steps ...

1. Write a brief description (less than 500 words) of the reasons this company or individual should be considered for an IDEA 01 Achievement Award. Be sure to indicate in which category it should be considered.

2. Gather together supporting materials — sales brochures, product samples, photos, newspaper or magazine articles, etc. — that will help the judges consider your nomination.

3. Send everything for arrival **BY NOVEMBER 15, 2000** to Michael Jacobsen, INDA Achievement Awards, 22 Paterson Avenue, Midland Park, NJ 07432. If appropriate, you can e-mail your nomination to mike@jacorpub.com or fax materials to 201-612-6677. Call 201-612-6601 with any questions.

• The more information on your nomination that you can provide the judges, the better!

• Yes, companies can nominate themselves.

• All entries will be judged by a special industry panel and three finalists in each category will be announced in NONWOVENS INDUSTRY and at www.nonwovens-industry.com and www.inda.org.